IDŐJÁRÁS

QUARTERLY JOURNAL
OF THE HUNGARIAN METEOROLOGICAL SERVICE

CONTENTS

****

http://www.met.hu/Journal-Idojaras.php

VOL. 117* NO. 2 * APRIL – JUNE 2013

IDŐJÁRÁS

Quarterly Journal of the Hungarian Meteorological Service

Editorial Office: Kitaibel P.u. 1, H-1024 Budapest, Hungary
P.O. Box 38, H-1525 Budapest, HUngary
E-mail: journal.idojaras@met.hu
Fax: (36-1) 346-4669

Indexed and abstracted in Science Citation Index Expanded™ and Journal Citation Reports/Science Edition
Covered in the abstract and citation database SCOPUS®

Subscription by mail:
IDŐJÁRÁS, P.O. Box 38, H-1525 Budapest, Hungary
E-mail: journal.idojaras@met.hu

IDŐJÁRÁS

Quarterly Journal of the Hungarian Meteorological Service
Vol. 117, No. 2, April – June, 2013, pp. 159–174

Ecological and economical impacts of climate change on Hungarian forestry practice

Ernő Führer[1], **Anikó Jagodics**[1], **István Juhász**[1], **György Marosi**[1], and **László Horváth**[2*]

[1]*Hungarian Forest Research Institute, Paprét 17, 9400 Sopron, Hungary*

[2]*Hungarian Meteorological Service, Gilice tér 39, 1181 Budapest, Hungary, and Plant Ecology Research Group of Hungarian Academy of Sciences at Institute of Botany and Ecophysiology, Szent István University, Páter K. utca 1, 2100 Gödöllő, Hungary*

**Correspondent author E-mail: horvath.l@met.hu*

(Manuscript received in final form March 12, 2013)

Abstract–As the result of the predicted climate change, not only the ecological circumstances but the profitability of forested areas will also change in the future in Hungary. The aim of this case study is to evaluate the expected ecological an economical impacts of a climate change scenario (REMO A1B) for three forest regions of Transdanubian Mountains (Bakony) for four climate indicator tree species (beech, hornbeam, sessile oak, and Turkey oak). According to this scenario, precipitation and air temperature increase by 5 percent and 1.3 °C, respectively in the spring months (March to May), while in summer (June to August) the precipitation decreases by 9 percent together with a higher temperature increase of 2.1 °C between the period of 2036 and 2065 compared to reference years (1961–2010). As a result of the forecasted climate change, a drift expected in forest climate classes towards the drier and warmer climate categories in Hungary, resulting in parallel decrease in production capacity of stands. We expect a significant area decrease in good forest yield classes together with an increase in poor categories. Hence, the annual revenues for the four indicator species will be lower by 9.4 percent compared to the reference period. The decrease in yield is caused by decrease of lumbered wood volume and more valuable wood assortments, as well. In case of the predicted climate scenario, the highest decay in production capacity will be expected for Turkey oak (12 percent), while the lowest for beech (7.5 percent).

Key-words: forest ecosystem, climate change, production capacity, forest yield classes, forest annual revenues

1. Introduction

The profitability of forestry practice is basically determined by ecological conditions beside the selection of tree species, the forestry practice applied, and the actual marketing circumstances (*Führer* and *Járó*, 1992). Namely, organic matter production of forests strongly depends on soil, hydrological, and climatic circumstances. While the quality of the first two site parameters can be considered as constant on short time basis, the climate, especially the magnitude and temporal variation of climate parameters show significant variability. Moreover, nowadays the change of climate can obviously be detected in Hungary, namely the climate becomes more and more warmer and drier as forecasted by *Bartholy et al.* (2009), *Faragó et al.* (2010), *Pieczka et al.* (2011), *Gálos et al.* (2007, 2012). In the forthcoming 50 years, frequency and strength of weather anomalies will be increasing. The evident, unfavorable changes in species composition, vitality, and growth of the forest ecosystems can be attributed to these changes according to numerous Hungarian forestry experts (*Berki et al.*, 2009; *Csóka*, 1996, 1997; *Csóka et al.*, 2007, 2009; *Czúcz et al.*, 2011; *Führer*, 1995; *Führer et al.*, 2011a,b; *Hirka* and *Csóka*, 2010; *Manninger*, 2004; *Mátyás*, 2010; *Mátyás* and *Czimber*, 2000, 2004; *Mátyás et al.*, 2010a,b, 2011; *Molnár* and *Lakatos*, 2009; *Solymos*, 2009; *Somogyi*, 2009; *Rasztovits et al.*, 2012).

Forestry, in practice, uses special climate categories represented by different tree species (*Járó*, 1972; *Führer*, 2010). These categories indicate different growing potential, therefore, any change in the area of climate categories accompanies with variation of organic matter production of the forest ecosystem (*Führer et al.*, 2011a,b). The forecasted warmer and drier climate in growing season would result in evident growth-loss of forest trees in Hungary; furthermore, a species composition change can also be expected on long-term time basis. The growth-loss can be indicated by the decrease in wood volume of an area unit. Considering that cost of logging are determined mainly by the actual marketing circumstances independently on climate change; final consequence of the loss in production will be the decrease of revenues and profitability of forestry practice.

The aim of this case study is to evaluate the expected ecological an economical impacts of a predicted climate change scenario for three forested regions of Transdanubian Mountains (Bakony) in Hungary (*Fig. 1*). In this work we investigate the climate of these state owned forests, the yield circumstances and potential revenues of climate indicator species, and the change of them as a result of climate change.

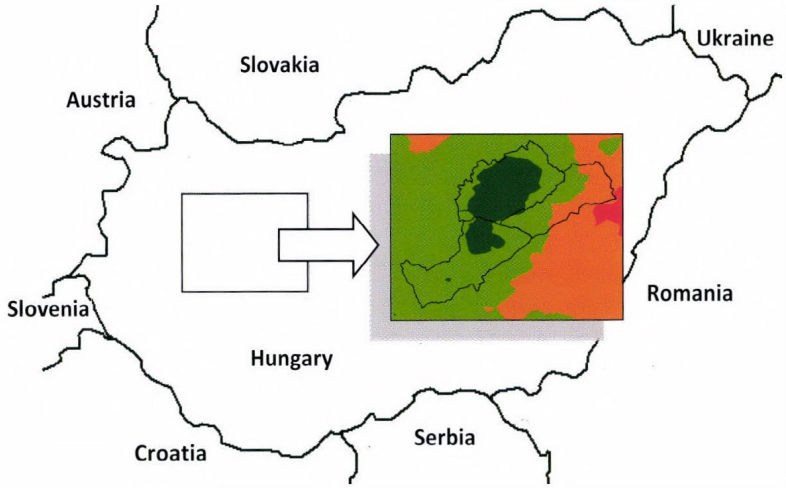

Fig. 1. Location of the three investigated forested regions in Hungary.

2. Methodology

The three forested test regions aimed in this study, in close connection each other, are the High-, South- and East-Bakony. Tough these areas are part of the same geographical region (Mountains), they can be characterized by a variety of ecological (pedology, hydrology, climate) circumstances. Altitude of these areas varies within 150 and 700 meters above sea level influencing among others the climate.

In the High-Bakony, the ratio of forested area is 53 percent (35,711 ha). Ridges of High-Bakony heighten over 600 m above sea level, however, nearly 48 percent of forests are located between altitudes of 350–450 m. Rate of forests between 450–550 meters is 15 percent, and above 550 m only 3.5 percent of forest can be found. Rate of forests below the altitude of 350 m above sea level mostly lies between 250 and 350 m; below that the share of forest does not reach the 3 percent. Dominant species are: beech (39 percent), hornbeam (15 percent), Turkey oak (14 percent), and sessile oak (4 percent).

In South-Bakony, the ratio of forests is 48 percent (31,989 ha). Forests can dominantly be found between altitudes of 150 and 450 m. Altitude distribution of forests are as follows, 150–250 m: 29 percent, 250–350 m: 34 percent, 350–450 m: 33 percent, and >450 m: 4 percent. Dominant species are: beech (12 percent), hornbeam (12 percent), Turkey oak (40 percent), and sessile oak (5 percent).

In the lower East-Bakony, the ratio of forested area is only 38 percent (18,132 ha). 42 percent of the forests lie between 250 and 350 m, accordingly to the lower altitude of this region. The ratios of forests below 250 m and above 350 m are 22 and 36 percent, respectively. Dominant species are: beech (9 percent), hornbeam (7 percent), Turkey oak (29 percent), sessile oak (8 percent), downy oak (12 percent), and European black pine (11 percent).

These data clearly show that the share of climate sensitive test species (as beech, hornbeam, Turkey oak, and sessile oak) is the highest in High-Bakony (72 percent), while the ratios of these in South-Bakony and East-Bakony are only 69 and 53 percent, respectively. In latter forest region, drought tolerant tree species (as downy oak, European black pine) significantly appear. While the share of beech (preferring highland, cool, moist climate) is the highest in High-Bakony (39 percent) and lowest in lower East-Bakony (9 percent), the pattern of sessile oak (preferring hilly, warmer climate) is just the opposite.

Respecting that the three regions range from 150 m up to 700 m above sea level, climate categories are definitely separated, caused by vertical changes. In the first stage of our evaluation we have characterized the climate of the regions mentioned above and the stands according to forestry climate classification methods (*Führer*, 2010; *Führer et al.*, 2011a, b) taking into account the growing circumstances of trees. The evaluation is based on precipitation and temperature data in those summer months when physiological processes are in intensive phase and 80–90 percent of organic matter production is realized (May to July) and in those (July, August) when growth of trees are limited by weather extremes. On the basis of meteorological data interpolated to the points of a Hungarian survey aiming the observation of forest stands growing (*Kolozs*, 2009) on a 2.8×2.8 km^2 grid, covering the regions, we have determined the distribution of different climate categories appeared in the examined forest regions by means of *forestry aridity index*, *FAI* (*Führer*, 2010; *Führer et al.*, 2011a) calculated from meteorological parameters in main growth cycle (May-July) and in critical months (July-August). *FAI* can be derived as:

$$FAI = 100 \times \frac{t_{VII-VIII}}{(p_{V-VII} + p_{VII-VIII})} \quad , \tag{1}$$

where $t_{VII-VIII}$ is the mean air temperature in critical months (July and August, °C), p_{V-VII} is the precipitation sum (mm) in the period from May to July, and $p_{VII-VIII}$ is the precipitation sum (mm) in the warmest (critical) months (July and August).

Then, we have collected the production capacities (from 1st to 6th forest yield classes) of state owned forests in different climate categories from the National Forest Database of Hungary, and we have evaluated the potential organic matter production in different climate categories. Test species

representing the forestry climate classes were involved in the evaluation, namely the beech (*Fagus sylvatica* L.), hornbeam (*Carpinus betulus* L.), sessile oak (*Quercus petraea* (Matt.) Liebl.), and Turkey oak (*Quercus cerris* L.).

Each forest yield class can be characterized by an annual average yield at the cutting age depending on tree species and actual marketing conditions. The change in yield of wood production and wood marketing is a suitable index for quantification of the economic impact of climate change. For this reason, in the economical evaluation we have determined the estimated yield of the test stands for each yield classes. Principle of the estimation was the yield of timber during wood harvesting operations in cutting cycle. Hence, revenues depend on the species, amount and quality of timber, and assortment composition. Respecting the available data for size and assortment composition of yield, separated for the target stands and for forest yield classes for the whole cutting cycle on the basis of previous investigations (*Márkus* and *Mészáros*, 2000; *Marosi et al.*, 2005), we have calculated the expected revenues. Annual rate of this parameter gives the mean revenues of the given yield class.

The economical influence of spatial realignment of the investigated stands, as a consequence of climate change, can be calculated by the method described above. Consequently, the product of the average annual yield of yield classes and area of the stand give the average yield of the given investigated forest stand.

We can estimate the change of this index in estimating the expected variation in area of different climate categories and the potential production capacity taking into account the climate scenarios. We have calculated with a climate change scenario, where the predicted changes in climate parameters to the reference climate period (1961–1990) are given for the period of 2036–2065. The scenario describes the expected changes in the investigated regions according to the A1B emission scenario of the REMO regional climate model (*Gálos et al.*, 2007). Hence, in the spring months (March to May) the precipitation and air temperature increase by 5 percent and 1.3 °C, respectively, while in summer (June to August) the precipitation decreases by 9 percent together with higher temperature increase of 2.1 °C compared to the period 1961–2010.

3. Results and discussion

3.1. Climate of studied forest stands

The Transdanubian Mountains (Bakony) have temperate cool and wet climate with prevailing wind of NW. In Hungary, forestry practice - depending highly on weather conditions - uses special climate classes; hence the different climate categories are represented by climate indicator test species. Accordingly, the coolest/most humid and warmest/most arid climates are represented by beech

and forest-steppe climate, respectively. In the middle there are hornbeam-oak climate close to *beech*, and sessile oak-Turkey oak close to forest-steppe climate. The yearly precipitation of originally treeless forest-steppe climate zones is not enough for production of native species, while sessile oak-Turkey oak climate is represented by these two species either together or separately. Precipitation and temperature characteristics of different climate categories are described in details by *Führer et al.* (2010, 2011a). On the basis of homogenized and interpolated meteorological data, the climate and the expected changes in different regions of Bakony can be characterized as follows.

In High-Bakony region the average yearly precipitation and the annual mean air temperature were 737 mm and 8.8 °C, respectively, between 1961 and 1990. Both are in the interval representative for beech climate (752±31 mm, 8.8±0.9 °C). The average temperature in the main growing period (16.1°C, May-July) and in critical months (18.0 °C, July-August) are lower than the averages of beech climate categories (16.6±0,8 and 18.5±0,8 °C). Precipitation amount for the same period (226 and 158 mm) are 10 and 5 percent lower than representative value for beech climate (259±13 and 167±9 mm). The main *FAI* for this region is 4.69 close to the upper limit of beech climate category (FAI_B: ≤4.75). On the basis of *FAI* calculated for the climate reference period (1961–1990) a total of 59 percent of this region lies in beech climate, while remaining part can be represented by hornbeam-oak climate (*Fig. 2*). In case of climate change according to the predicted scenario, the mean of *FAI* increases up to 5.59 hence there will be no longer beech climate in that region, moreover, 13 percent of the High-Bakony will be represented by sessile oak-Turkey oak climate.

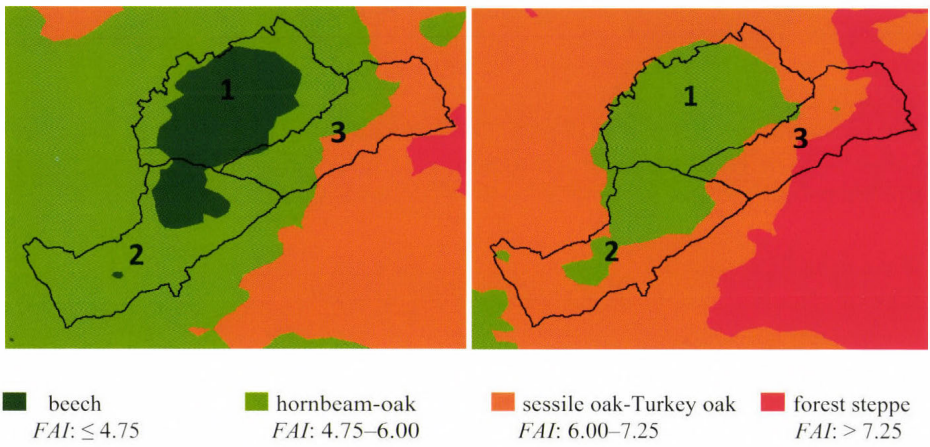

Fig. 2. Distribution of climate classes according to *FAI* in the examined forest regions; left: in the reference years (1961–1990), right: in case of the predicted scenario.

In the South-Bakony region, the average yearly precipitation and the annual mean air temperature were 693 mm and 9.4 °C, respectively, between 1961 and 1990 corresponding to the averages of hornbeam-oak climate (663±55 mm, 9.4±0.7 °C). Average temperature in the main growing period (May-July) is 16.7°C, while in the critical months it is 18.6 °C, i.e., temperature circumstances are representative rather for the cooler *beech* climate. However, precipitation data in the same period (219 and 150 mm) is representative again for hornbeam-oak climate (218±15 and 139±13 mm). For this region the *FAI*, as an overall index, is 5.03 refering to the hornbeam-oak climate (4.75–6.00). The share the climate classes here is 20 percent beech and 80 percent hornbeam-oak. In case of climate change scenario, the predicted average *FAI* increases up to 5.98, which is practically at the borderline between the hornbeam-oak and the sessile oak-Turkey oak climates. In this case, 44 percent of the region would be representative for hornbeam-oak and the remaining part to the sessile oak-Turkey oak climate. On the basis of this prediction, total extinction of beech zone is expected (*Fig. 2*).

In the East-Bakony region, the average yearly precipitation and the annual mean air temperature were 634 mm and 9.3 °C, respectively, between 1961 and 1990. These values are close to hornbeam-oak climate (663±55 mm, 9.4±0.7 °C), similarly to the average temperature in main growing period (17.3 °C) and in critical months (19.4 °C). On the other hand, the precipitation amount in these months are lower (198 and 132 mm) than favorable for hornbeam-oak climate (218±15 and 139±13 mm). Average *FAI* in this region is 5.88 close to the borderline between the hornbeam-oak and sessile oak-Turkey oak climates (6.00). The share of the beech, hornbeam-oak, and sessile oak-Turkey oak climates in this region is 2, 51, and 47 percent, respectively (*Fig. 2*). In case of the predicted climate scenario, the average *FAI* changes to 6.95 and the share of different climate categories would change to hornbeam oak: 9, sessile oak-Turkey oak: 51, and forest steppe: 9 percent ratios.

Average *FAI* for the total areas of the three regions (High-, South-, and East-Bakony) in the reference years is 5.09, lying in the favorable side of hornbeam-oak climate (close to the beech climate). This value would change to 6.05 (nearly by one *FAI* unit) in case of the predicted climate scenario. It means that, in the area of the three regions, 30 percent of beech climate would disappear, the share of hornbeam-oak climate would decrease from 58 to 52 percent; the ratio of sessile oak-Turkey oak climate would increase from 12 to 32 percent, while forest steppe climate would appear sharing 10 percent in the region.

The total surface area of the three Bakony regions is 179,621 ha; ratio of forested areas is 48 percent (85,752 ha). In our study only the state owned forests (64,957 ha) are involved, where the share of beech, hornbeam-oak, and sessile oak-Turkey oak climates are 36, 57, and 7 percent, respectively. Classification of the Forest Database (*MGSZH*, 2008) based on climate indicator

tree species differsfrom our results: the share of the climate is 41 percent beech, 33 percent hornbeam-oak, and 26 percent sessile oak-Turkey oak climate (*Table 1*).

Table 1. Distribution of forest yield classes according to the forest management plan and the *FAI* for state owned forests in the examined regions (in percent)

climate classes	**High-Bakony**		**South-Bakony**		**East-Bakony**		**Bakony**	
	plan	*FAI*	plan	*FAI*	plan	*FAI*	plan	*FAI*
beech	78	67	17	23	15	3	41	36
hornbeam-oak	21	33	44	77	36	70	33	57
sessile oak-Turkey oak	1	0	39	0	49	27	26	7

Regarding this distribution in lower scale, the differences are higher. In High-Bakony, 78 percent of the state owned forest are in beech zone, followed by hornbeam-oak climate (21 percent) and the ratio of sessile oak-Turkey oak climate is only 1 percent. In contrast in South-Bakony, hornbeam-oak climate is the dominant (44 percent), while ratio of sessile oak-Turkey oak and beech climates is 40 and 16 percent, respectively. In the East-Bakony region, the share of climate zones is: 49 percent of sessile oak-Turkey oak, 36 percent of hornbeam-oak, and only 15 percent of beech.

Classification according to forestry aridity index (FAI, Eq. 1) differs from figures above. Taking into account the period of 1961-1990 as reference, the ratio of the beech climate in High-Bakony, South-Bakony, and East-Bakony are 67, 21, and 2 percent respectively. The ratio of the hornbeam-oak climate is highest in South-Bakony (77 percent), a little lower in East-Bakony (71 percent), while in High-Bakony it is only 33 percent. Significant share of sessile oak-Turkey oak climate can be found in East-Bakony (27 percent).

It seems that the difference between the two classifications is lower for High-Bakony with cooler and wet climate, compared to the other two drier and warmer Bakony regions (*Table 1*). Remarkable, that for latter regions the sessile oak-Turkey oak climate shares significant areas according to the forest management classification plan (South-Bakony 39; East-Bakony 49 percent). Explanation for this is that in forestry practice, the sessile oak-Turkey oak climate was classified according solely to the Turkey oak species. In contrast, nowadays, owing to the appropriate forestry practice the majority of Turkey oak trees can be found in hornbeam-oak climate zones. Reasons can be traced back to the practice in the 19th and 20th centuries, when two of the main aims were to satisfy the rapidly increasing firewood demand and the utilization of rich acorn yield as mast (rearing of pigs).

The difference between the two classifications underlines the necessity that the data in Forest Database – possible subjects of modification according to the

actual species selection policy – must be supervised in the future. It is also important, since the reference basis in evaluation of impact of expected climate change in connection to tree species may have high influences to the outcome, i.e., the measure of changes.

3.2. Composition of production capacity of regions and its change according to the predicted climate scenario in state owned forests

3.2.1. Production capacity of tree species of different regions

Wood production capacity of a given site is characterized by the sum of annual average growth calculated up to the critical cutting age, and it can be classified into good (1st and 2nd), medium (3rd and 4th), and poor (5th and 6th) classes. On the basis of the Forest Database, the investigated regions can be characterized as follows, good: 24, medium: 40, and poor: 36 percent (MGSZH 2008) (*Fig. 3*). More favorable conditions are in High-Bakony, where share of classes 1st and 2nd is 46 percent, in contrast with other two regions where only 8–9 percent of trees are in the good classes. In East-Bakony, 65 percent of trees are in the poor category, where circumstances for production are less favorable mainly due to the unfavorable, climate for the given species composition. In South-Bakony, the majority of stand belongs to the medium (48 percent) and poor (43 percent) categories.

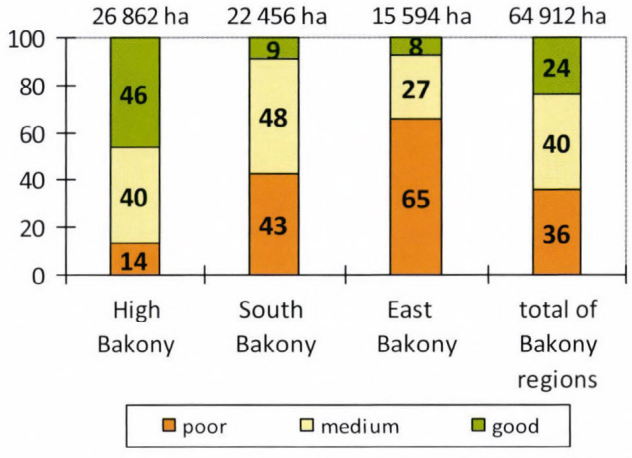

Fig. 3. Distribution of forest yield classes in the *Bakony* regions (in percent).

On the basis of distribution of forest yield classes (from 1st to 6th), the calculated average production capacity index (average of area weighted yield classes) in High-Bakony is 3.1, in South-Bakony its value is 4.2 due to the more unfavorable ecological conditions, and it is the worst in East-Bakony (4.9), as a

consequence of most unfavorable conditions in this region. It is evident, because the share of different climate categories differs for the different regions (*Table 2*), and the production capacities of climate categories are also different (beech climate: 2.9, hornbeam-oak climate: 4.3, and Turkey oak- sessile oak climate: 5.1).

Respecting the large differences among the climate conditions for the different investigated regions, we have examined whether these differences appear in production capacity of test species. Area covered by test species in the state owned forests is 44,884 ha, with largest share of Turkey oak (17,941 ha), followed by beech (15,459 ha), hornbeam (7,516 ha), and sessile oak (3,968 ha).

It is evident, that among the three regions the structure of forest yield classes of test species is most favorable in High-Bakony, where the share of good class is the highest, while poor categories represent the lowest area (*Fig. 4*). Conversely, the worst conditions are in East-Bakony. Average production capacity index for beech is 2.5, 3.1, and 3.3 in High-, South-, and East-Bakony, respectively. Difference among regions is higher in case of Turkey oak, where indices for the regions above are 3.3, 4.3, and 5.0. For all of four test species the difference is larger between High- and South-Bakony than between South- and East-Bakony, showing that climate of latter two regions are closer and highly differs from that of High-Bakony. Average tree production capacity index for the group of three regions is the lowest for beech (2.6), followed by hornbeam (3.5), sessile oak (4.0), and Turkey oak (4.2).

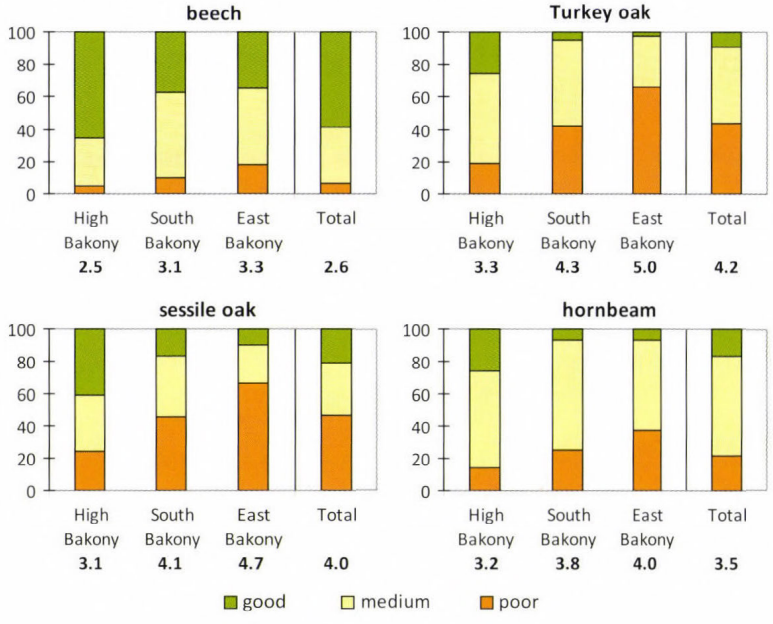

Fig. 4. Structure of forest yield classes in the examined regions (in percent).

3.2.2. Expected change in production capacity of test species for the examined regions

As it was mentioned above, four test species only in areas of state owned forests were involved in evaluating the change of area of climate classes according to the predicted climate scenario. Share of state owned forests in the three regions is 52 percent. On the basis of evaluation, the ratio of good yield classes decrease in the direction from beech to sessile oak-Turkey oak climate for four test species (*Fig. 5*). Ratio of stands in poor categories is considerably increased for hornbeam, sessile oak, and Turkey oak. For beech in Turkey oak climate, even the ratio of medium category remarkably increases as well. Certainly, the effect of climate involving the effectiveness of precipitation is influenced by the properties of underlying soil in high extent. E.g., there are stands in poor class in soils with thin organic layer or with wrong mechanical parameters even in favorable climate conditions; and vice versa, stands over deeper and better structured soils can utilize the precipitated water effectively, increasing the organic matter production.

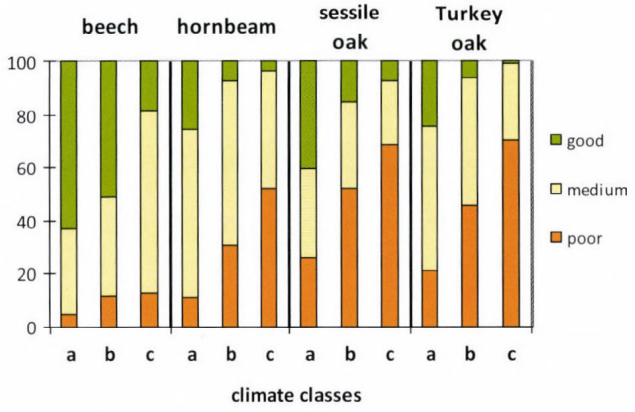

Fig. 5. Distribution of climate indicator tree species in the climate classes according to forest yield classes (in percent). Climate classes: a= beech, b=hornbeam-oak, c=sessile oak-Turkey oak.

By means of the aridity index (*FAI*), we can predict that majority of *beech* climate –calculated using the basic climate reference period (1961–1990) – will be moved to hornbeam-oak climate as a consequence of even a minor summer temperature increase at the examined three Bakony regions. According to the predicted scenario, when higher temperature increase and minor decrease in precipitation amount can be expected in summer season, the beech climate completely disappears, all of them will be moving towards hornbeam-oak climate. In turn, half area of former hornbeam-oak climate will be dominated by Turkey oak climate. Accordingly, the climate dependent tree production

capacity most likely changes; pattern of forest yield class of beech climate declines to hornbeam-oak, while latter declines to sessile oak-Turkey oak climate (*Fig. 6*). Namely, we can expect a decrease in production capacity of stands, even at constant soil properties; i.e., area of good production capacity decreases from 12,781 to 5,058 ha, together with an increase of poor area from 12,339 to 21,401 ha.

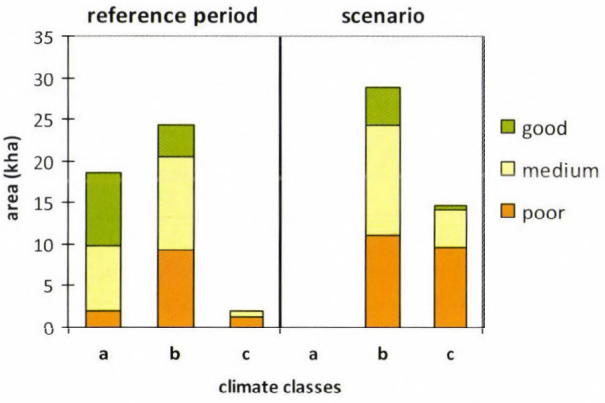

Fig. 6. Distribution of forest yield classes in climate classes in the reference period (1961–1990) and in case of predicted scenario. Climate classes: a= beech, b=hornbeam-oak, c=sessile oak-Turkey oak.

3.2.3. Yield indices of test species and their change in the investigated forest regions

It can be clearly seen from the specific revenues of forest yield classes calculated for the four climate indicator tree species (beech, hornbeam, Turkey oak, and sessile oak), that revenues for beech and sessile oak in good (1st and 2nd) classes is remarkably higher than that of for hornbeam and Turkey oak (*Marosi et al.*, 2005) (*Table 2*).

Table 2. Average revenues of forest yield classes for each climate indicator tree species (in kHUF ha^{-1} $year^{-1}$) (*Marosi et al.*, 2005)

yield classes	beech	hornbeam	sessile oak	Turkey oak
1st	129	55	129	62
2nd	108	46	108	53
3rd	77	37	83	42
4th	62	29	68	35
5th	43	21	51	25
6th	29	16	37	19

From the point of view of wood industry, the beech and oak are much more valuable than the hornbeam and Turkey oak, however the difference is continuously decreasing to the direction of less favorable ecological circumstances, more in case of beech and less for sessile oak. As previous investigations in Hungary have shown, stands in poor yield classes (5th and 6th) still do not produce any profitability.

For the 45 kha of state owned forests in the three Bakony regions, based on revenues concerning to different yield classes, we have estimated the expected economical effect of the climate change according to the forecasted scenario. As it has already been demonstrated, the expected climate change reduces the production capacity of forests. In practice, it appears in the change of the ratio of different forest yield classes. Area of good classes significantly decreases with parallel increase of poor classes, hence, available revenues decreases accordingly, as lumbered wood volume and the ratio of more valuable wood assortments decrease as well (*Fig. 6*). Specific expenses of forest management do not change significantly hence the fewer revenues appear in the decrease of profitability. In this study we disregard the case when ecological changes require the change (replace) of tree species. Naturally, in this case as a consequence of further increase of expenses, profitability would be even less depending on kind of tree species and on the technology applied.

Referring the average change of revenues to ha unit, it is highest for sessile oak (7.893 kHUF ha^{-1}, followed by beech (6.941 kHUF ha^{-1}), hornbeam (4.098 kHUF ha^{-1}), and Turkey oak (3.920 kHUF ha^{-1}) (*Fig. 7*).

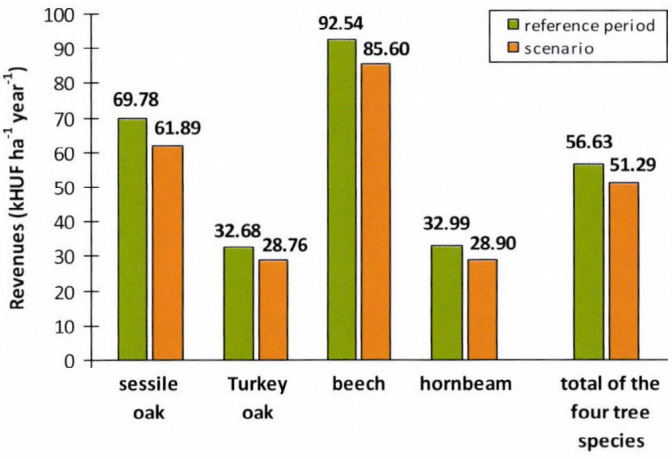

Fig. 7. Average annual revenues of test species in the examined forest regions in the reference period (1961–1990) and in case of the predicted scenario.

Calculating with the scenario predicted, the revenues will be lower by 9.4 percent for the four test species. It means that the state forest companies expect only 2.302 billion HUF (10.56 million USD) instead of 2.542 billion HUF (11.66 million USD) in the 45 kha area for the middle of this century, at the present price level. This rate of deficit may query the profitability of forest management. The four test species respond to the climate changes in different extent; highest deficit can be expected for Turkey oak and lowest for beech.

4. Conclusions

The predicted climate change probably influences the profitability of forest management besides the ecological circumstances of forested areas. We have estimated the expected changes to the A1B climate scenario for the case of test species locating in a group of Hungarian forest regions (High-, South-, and East-Bakony). The average measure of the predicted scenario between years of 2036–2065 compared to the reference period (1961–1990) is the follows: in the spring months (March-May) the precipitation decreases by 5 percent, the air temperature increases by 1.3 °C, while in the summer months (June-August) the precipitation decreases by 9 percent parallel with a dramatic temperature increase of 2.1 °C.

The average calculated forestry aridity index (*FAI*) for the three investigated Bakony regions in the reference period (1961–1990) is 5.09 favoring to hornbeam-oak climate. In these areas the dominating climate zones are *beech* (36 percent), hornbeam-oak (57 percent), and sessile oak-Turkey oak (7 percent) (*Fig. 2*).

On the basis of the predicted scenario, *FAI* increases to 6.05 extremely enlarging the share of sessile oak-Turkey oak zones dominating in East-Bakony, while hornbeam-oak climate will be representative in High-Bakony. In South-Bakony, hornbeam-oak and sessile oak climates will equally be characteristic.

As to the productivity we find the best conditions in High-Bakony (*Fig. 3*), where the ratio of good yield classes is higher, in contrast with the two other regions, where good classes share the lowest ratio of areas. Two-third of East-Bakony areas belong to the poor yield classes.

According to the assessment of climate, classes the ratio of good classes definitely decreases from beech to sessile oak climate in case of four climate indicator species (*Fig. 4*). At the same time, the share of poor yield classes significantly increases for hornbeam, sessile oak, and Turkey oak.

As a response to climate change – according to the scenario discussed – we expect a shift in climate classes resulting in decay in production capacity even at constant soil conditions, i.e., share of good classes decreases with parallel increase of poor classes.

For the four climate indicator tree species, the annual average revenues will be lower by 9.4 percent compared to the reference period in the forecasted interval (*Fig. 7*). There are two reasons of that, on one hand the volume of yield, and on the other, the ratio of valuable assortments will also be lower.

The respond of four species are different. In the case of predicted climate scenario, the highest decay in production capacity will be expected for Turkey oak (12 percent), while the lowest for the beech (7.5 percent).

Expected unfavorable ecological effect of climate change can be a high risk for forest management. Today, the conservation of forests can be financed exclusively by revenues of selling wood products on the market. If the revenues decrease as calculated above and there will not be other available sources to finance then the steady maintenance of forests will be questionable in lack of profitability of forest management.

Acknowledgements–our research was supported by NKTH-OTKA_A_08-2-2009-0054 (80305-80335) and by the TÁMOP-4.2.2/08/1-2008-0020 projects.

Refrences

Bartholy, J., Pongrácz, R., Torma, Cs., Pieczka, I., Kardos, P., and *Hunyady, A.,* 2009: Analysis of regional climate change modelling experiments for the Carpathian basin. *Int J Glob Warming 1*, 238–252.

Berki, I., Rasztovits, E., Móricz, N., and *Mátyás, Cs.*, 2009: Determination of the drought tolerance limit of beech forests and forecasting their future distribution in Hungary. *Cereal Res. Commun. 37*, 613–616.

Czúcz., B., Gálhidy, L., and *Mátyás, Cs.*, 2011: Present and forecasted xeric climatic limits of beech and sessile oak distribution at low altitudes in Central Europe. *Ann. For. Sci. 68*, 99–108.

Csóka, Gy., 1996: Aszályos évek – fokozódó rovarkárok erdeinkben. *Növvéd 32*, 541–551.(in Hungarian)

Csóka, Gy., 1997: Increased insect drought impact damage in Hungarian forests under drought impact. *Biologia 52*, 159–162.

Csóka, Gy., Koltay, A., Hirka, A., and *Janik, G.*, 2007: Az aszályosság hatása kocsánytalan tölgyeseink és bükköseink egészségi állapotára. In (*Mátyás Cs., Vig P.* (Eds.)), Proceedings of the 5th Forests and Climate Conference, Nyugat-Magyarországi Egyetem, Sopron, 229–239.

Csóka Gy., Koltay A., Hirka A., and *Janik G.,* 2009: Az aszályosság hatása kocsánytalan tölgyeseink egészségi állapotára. *„KLÍMA-21" Füzetek 57*, 64–73. (in Hungarian)

Faragó T., Láng I., and *Csete L.* (Eds.) 2010: Climate Change and Hungary: Mitigating the Hazard and Preparing for the Impacts (the „VAHAVA" Report http://www.unisdr.org/files/18582_thevahavareport08dec2010.pdf

Führer E., 1995: Az idôjárás változásának hatása az erdők fatermő képességére és egészségi állapotára. *Erd Lapok 130*, 176–178. (in Hungarian)

Führer, E., 2010: A fák növekedése és a klíma. *„KLÍMA-21" Füzetek 61*, 98–107. (in Hungarian)

Führer, E. and *Járó, Z.,* 1992: Auswirkungen der Klimaänderung auf die Waldbestände Ungarns. *Österreichische Forsztg 9,* 25–27.

Führer, E., Mátyás, Cs., Csóka, Gy., Lakatos, F., Bordács, S., Nagy, L., and *Rasztovits, E.*, 2010: Current status of European beech (*Fagus sylvatica* L.) genetic resources in Hungary. *Communicationes Instituti Forestalis Bohemicae 25*, 152–163.

Führer, E., Horváth, L., Jagodics, A., Machon, A., and *Szabados, I.,* 2011a: Application of a new aridity index in Hungarian forestry practice. *Időjárás 115*, 103–118.

Führer, E., Marosi, Gy., Jagodics, A., and *Juhász, I.* 2011b: A klímaváltozás egy lehetséges hatása az erdőgazdálkodásban. *Erdtud. Közl. 1*, 17–28. (in Hungarian)

Gálos, B., Lorenz, Ph., and *Jacob, D.,* 2007: Will dry events occur more often in Hungary in the future? *Envir Res Lett 2*, 034006.

Gálos, B., Mátyás, Cs., and *Jacob, D.*, 2012: Az erdőtelepítés szerepe a klímaváltozás hatásának mérséklésére. *Erdtud Közl 2*, 35–45. (in Hungarian)

Hirka, A. and *Csóka, Gy.*, 2010: Abiotikus károk Magyarország erdeiben. *Növvéd. 46*, 513–517.

Járó, Z., 1972: Az erdészeti termőhelyértékelés rendszere. In (*Danszky, I.* (Ed.)) Erdőművelés. Mezőgazdasági Kiadó, Budapest, 47–256. (in Hungarian)

Kolozs, L., (Ed.) 2009: *Erdővédelmi Mérő- és Megfigyelő Rendszer (Emmre) 1988–2008*. MGSZH Központ Erdészeti Igazgatóság, Budapest, Hungary, 1–161. (in Hungarian)

Manninger, M., 2004: Erdei fák éves és korszaki növekedésmenete és kapcsolódása egyes ökológiai tényezôkhöz In (*Mátyás, Cs.* and *Vig, P.*, (Eds.)), Proceedings of the 4th Forests and Climate Conference, Nyugat-Magyarországi Egyetem, Sopron, 151–162.

Márkus, L., and *Mészáros, K.*, 2000: Erdőérték-számítás. Mezőgazdasági Szaktudás Kiadó, Budapest. (in Hungarian)

Marosi, Gy., Solymos, R., Rédei, K., Führer, E., Molnár, S., Pásztory, Z., and *Juhász, I.*, 2005: A fatermesztés és faanyaghasznosítás modelljeinek kidolgozása célállományonként.. In (*Molnár, S.*, (Ed.)) Erdő-fa hasznosítás Magyarországon. Nyugat-Magyarországi Egyetem, Faipari Mérnöki Kar, Sopron, 377–386. (in Hungarian)

Mátyás, Cs., 2010: Forecasts needed for retreating forests. *Nature 464*, 1271.

Mátyás, Cs. and *Czimber, K.*, 2000: Zonális erdőtakaró mezoklíma szintű modellezése: lehetőségek a klímaváltozás hatásainak előrejelzésére. In (*Tar, K.*, (Ed.)) Proceedings of the 3rd Forests and Climate Conference, Debreceni Egyetem, Debrecen, 83–97. (in Hungarian)

Mátyás, Cs. and *Czimber, K.*, 2004: A zonális alsó erdôhatás klímaérzékenysége Magyarországon – előzetes eredmények. In (*Mátyás, Cs.* and *Vig, P.* (Eds.)) Proceedings of the 4th Forests and Climate Conference. Nyugat-Magyarországi Egyetem, Sopron, 35–44.

Mátyás, Cs., Berki, I., Czúcz, B., Gálos, B., Móricz, N., and *Rasztovits, E.*, 2010a: Future of beech in Southeast Europe from the perspective of evolutionary ecology. *Acta Silvatica et Lignaria Hungarica 6*, 91–110.

Mátyás, Cs., Führer, E., Berki, I., Csóka, Gy., Drüszler, Á., Lakatos, F., Móricz, N., Rasztovits, E., Somogyi, Z., Veperdi, G., Vig, P., and *Gálos, B.* 2010b: Erdők a szárazsági határon. *„KLÍMA-21" Füzetek 61*, 84–97. (in Hungarian)

Mátyás, Cs., Berki, I., Czúcz, B., Gálos, B., Móricz, N., and *Rasztovits, E.* 2011: Assessment and projection on climate change impacts in SE European forests. a case study of common beech (*Fagus sylvatica* L.). *Revija za Lesno Gospodarstvo 63*,142–153.

MGSZH, 2008: Országos erdőadattár 2006. 01. 01. állapot. MGSZH Központ Erdészeti Igazgatóság, Budapest, Hungary (CD-ROM edition). (in Hungarian)

Molnár, M. and *Lakatos, F.*, 2009: A bükkpusztulás Zala megyében – klímaváltozás? *„KLÍMA-21" Füzetek 57*, 74–82. (in Hungarian)

Pieczka, I., Pongrácz, R., and *Bartholy, J.*, 2011: Comparison of simulated trends of regional climate change in the Carpathian Basin for the 21st century using three different emission scenarios. *Acta Silvatica et Lignaria Hungarica 7*, 9–22.

Rasztovits, E., Móricz, N., Berki, I., Pötzelsberger, E., and *Mátyás, Cs.*, 2012: Evaluating the performance of stochastic distribution models for European beech at low-elevation xeric limits. *Időjárás 116*, 173–194.

Solymos, R., 2009: A klímaváltozás hatása az erdők fanövedékére. *„Klíma-21" Füzetek 56*, 43–47. (in Hungarian)

Somogyi, Z., 2009: A klíma, a klímaváltozás és a fanövekedés néhány összefüggése. *„Klíma-21" Füzetek 56*, 48–56. (in Hungarian)

IDŐJÁRÁS

Quarterly Journal of the Hungarian Meteorological Service
Vol. 117, No. 1, April–June 2013, pp. 175–186

Regional differences between ambient temperature and incidence of Lyme disease in Hungary

Attila Trájer[1*], **János Bobvos**[2], **Katalin Krisztalovics**[3], and **Anna Páldy**[2]

[1*]*Semmelweis University, Budapest, Hungary*
1085 Budapest, Üllői str. 26.

[2]*National Institute of Environmental Health, Budapest, Hungary*
1097 Budapest, Gyáli str. 2–6.

[3]*National Centre of Epidemiology, Budapest, Hungary*
1097 Budapest, Gyáli str. 2–6.

**Corresponding author E-mail: trajer.attila@oki.antsz.hu*

(Manuscript received in final form December 18, 2012)

Abstract–The regional climate impacts on Lyme borreliosis (LB) or Lyme disease have not been studied yet in Hungary. By this study we want to contribute the assessment of the impact of climate change on vector-borne diseases. Our aim was to assess the influence of regional spatial-temporal differences of annual temperature conditions, as well as the start of the vegetation season on LB. We created climatic contrast by selecting three southwestern (Zala, Somogy, Baranya; henceforth: SW) and two northeastern (Nógrád and Borsod-Abaúj-Zemplén: NE) counties in Hungary. Weekly LB data and the site of infection on county level for 1998–2010 were gained from the National Epidemiologic and Surveillance System. The temperature data were retrieved from the European Climate Assessment and Dataset. The regional differences of the weekly LB incidence were studied in relation to regional temperature differences. Descriptive statistics, linear and polynomial regression models were applied.

We observed a 1.6 °C difference in the mean winter temperatures between the two regions: the mean winter temperature of the NE counties was under 0 °C, in the SW counties it was more than 1 °C. In the SW counties spring warming started 2 weeks earlier, and there were only 3 weeks in the year, when the weekly mean temperature sank below 0 °C by few tenths of a degree. In the NE counties, this period lasted for 8 weeks continuously.

The first day with mean temperature of 10 °C followed by days with mean temperature >8 °C was chosen as start of spring. Based on this criterion and according of a linear regression model, in 2010 spring started by 2.5 weeks earlier in the two NE counties, less than 1 week earlier in the three SW counties compared to the beginning year of 1998. A difference of 3 weeks was observed in the detection of 10 cases of LB per week between the 2 NE and 3 SW counties, and there was a 3-4 weeks difference between the annual LB maxima. Comparing the periods of 1998–2003 and 2005–2010, the peak of the LB season sifted from the 28th to the 29th weeks in the NE counties, while in the SW counties this

shift did not reach one week difference. In the NE counties, the cumulative LB incidence showed a 25.68 % increase in periods 1999–2004 and 2005–2010 in the SW counties the same increase was 30.55%.

Key-words: Lyme borreliosis, regional climatic differences, *Ixodes ricinus,* indicator species, vector-borne disease, climate change

1. Introduction

Lyme borreliosis (LB) is one of the most common vector-borne diseases in Europe. Due to the environmental sensitivity of the species of the *Ixodes* genus, these organisms and tick-borne diseases are one of the most useful climate or climate change indicators for the Northern Hemisphere (*Brownstein et al.*, 2005*; Donnelly et al.*, 2004; *English et al.*, 2009*; Kovats*, 2003; *Lindgren* and *Jaenson*, 2006;). The arthropod vectors and consequently, the vector-borne diseases are also sensitive to climatic conditions (*Rogers* and *Randolph*, 2006).

Lyme borreliosis (LB) is the most common arthropod-borne human infection in Hungary. The geographic distribution is a very important characteristic of the host and vector populations and the human transmission of LB (*James et al.*, 2010). *Stafford et al.* (1998) found that the incidence of Lyme disease positively correlated with tick abundance which showed an increasing tendency since the 1990's in Europe (*Randolph* , 2004; *Confalonieri*, 2007). In Hungary, as in Western Europe, *Ixodes ricinus* Linnaeus (1758) is the main vector of LB, but *Dermacentor reticulatus* Fabricius (1794) is a common vector tick as well (*Földvári et al.*, 2007).

As a kind of external parasites, the complex three-stage onthogeny of *Ixodes* ticks occurs in the environment, the spatial-temporal distribution of ticks in the nature depends on climatic and ecologic conditions (*Estrada-Pena,* 2008). *Kalluri et al.* (2007) discovered a strong seasonal association between the time of the annual maximum of weekly LB incidences occurring during the summer and fall months, when the nymphs are most active and the seasonal temperature and precipitation change. *Duffy* and *Campbell* (1994) found that 4 °C was the threshold of the activity of *Ixodes scapularis* Say (1821) in the milder winter days. According to *Lindgren* and *Gustafson* (2001), the threshold temperature of questing (food-seeking) tick activity was at 7–8 °C, *Perret et al.* (2000) came to a very similar conclusion (between 6.6 and 8 °C). Ambient temperature is one of the most important factors of the tick activity mainly in spring (when the relative humidity and soil moisture are appropriate for the ticks), but to explain the absolute annual LB case number, the ambient temperature is insufficient.

For the prediction of the expected effects of the future climate change on LB, it is essential to study the existing geographical differences in the LB seasons to investigate the weekly, cumulative LB incidence rates based on the present regional climate differences, and to observe the probable different seasonality of LB by regions. In our study we aimed at these observations.

2. Data and methods

2.1. Data and statistics

The weekly data of LB for 1998–2010 were retrieved from the National Epidemiologic and Surveillance System. The daily temperature data in 25 km grids are from the European Climate Assessment and Dataset (*Tank et al.,* 2002; *Haylock et al.*, 2008). Regional differences in the weekly LB incidence were studied in two northeastern and three southwestern counties in Hungary. In our study we used descriptive statistics, and the associations were analyzed by linear and polynomial regression models using SPSS 10.0 software.

2.2. Selection of the studied counties

We selected counties with similar level of forestation, number of inhabitants, and order of LB incidence. The cumulative number of population of the three southwestern (SW) counties (Zala, Somogy, Baranya) was 1,002,977 inhabitants in 2010 and the number of population of the northeastern (NE) counties (Nógrád, Borsod-Abaúj-Zemplén) was 897,688 inhabitants (*KSH*, 2010) in the same year (2010). To calculate the LB incidences we used the population numbers of 2010. The population ratio of the NE/SW counties was 0.895 – a slight difference (10.5%) exists between the two study regions.

The mean forestation of the 3 SW counties (27.74%) and the forest cover of the 2 NE counties (32.70%) are very similar, only a 15.16% difference exists (*Komarek*, 2005).

The difference between the cumulative LB incidences in period 1998–2010 of the 2 regions is not too high (NE counties: 298.99/ 100.000 and SW counties: 244.73/ 100.000), 18.2% difference exists. So, the difference of the mean forestations and the cumulative LB incidences was similar: 15.16% – 18.2% for the 13-year period.

3. Results

3.1. Differences between the weekly ambient temperatures

The comparison of the monthly mean temperature of the 3 southwestern and 2 northeastern counties (*Fig. 1*) in period 1998–2010 showed differences mainly in winter, early spring, and autumn seasons. The biggest difference was that in the southwestern counties, the January mean temperature did not exceed the 0 °C limit (*Fig. 2*). In the case of Zala, Baranya, and Somogy counties (SW), the winter was milder than in the NE counties. While in the SW counties the mean weekly temperature of winter months fluctuated near 0 °C, in the NE counties it sank to between –1 and –2 °C. The two curves met at the 13th week of the year. The

mean summer temperatures were the same in both regions, althought the autumn was milder in the SW counties. From November to the end of March, the weekly mean temperature differences of the examined 13 years reached 1 °C.

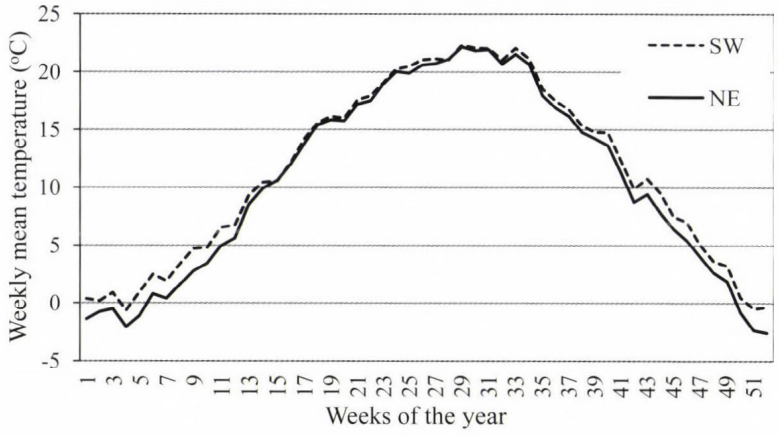

Fig. 1. Weekly mean ambient temperatures in the SW and NE counties in Hungary, in 1998–2010.

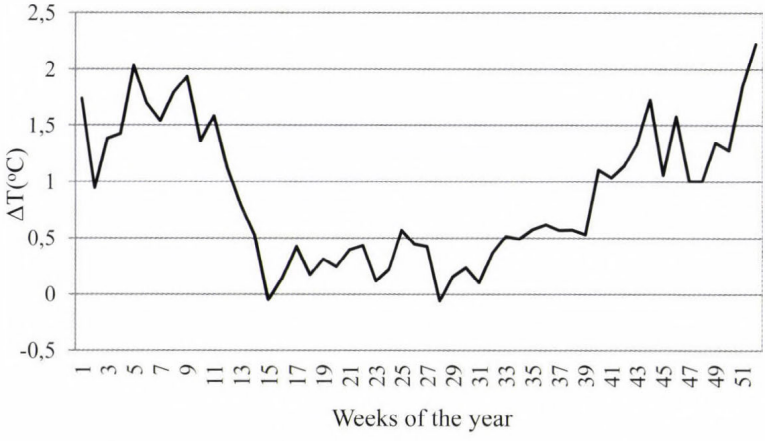

Fig. 2. Differences in the weekly mean temperatures between the SW and NE counties in Hungary, in 1998–2010.

The mean winter temperature was 1.2 °C in the 3 southwestern counties in period 1998–2010, respectively it was –0.3 °C in the 2 NE counties, the difference was 1.6 °C with a dispersion of 1.1 °C (*Fig. 3*). Due to the similar

climatic influence and the small geographical distance (the nearest distance is about 100 km and the greatest distance is about 400 km), the correlation between the mean winter temperatures of the two regions was very strong ($R^2=0.9554$, $P<0.0001$; *Fig. 4*).

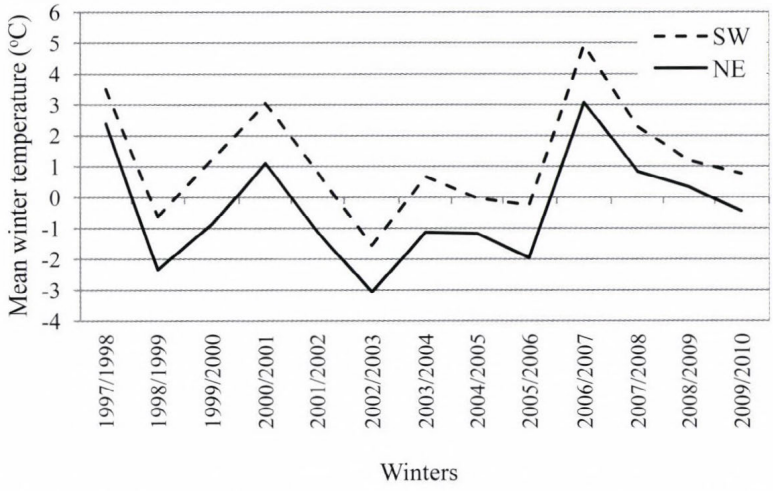

Fig. 3. Mean winter temperatures in the SW and NE counties in Hungary, in 1998–2010.

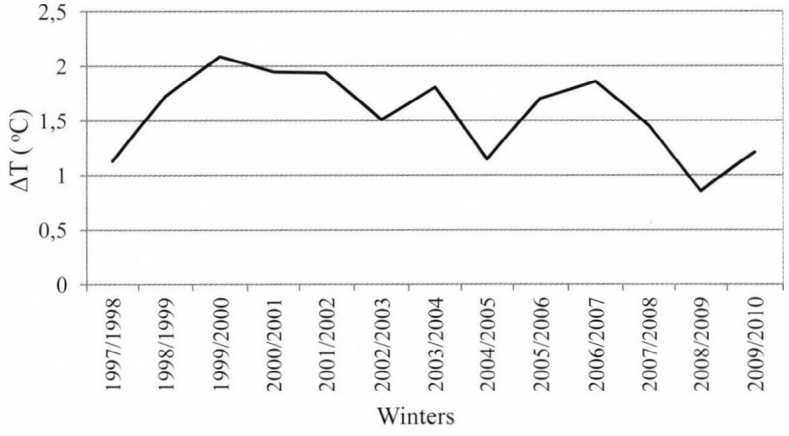

Fig. 4. Differences in the mean winter temperatures between the SW and NE counties in Hungary, in 1998–2010.

3.2. The shift of the start of the LB season

Our previous observations showed that the incidence rate of 0.1/100.000 is a good indicator of the onset of LB season, and usually coincides with the first stable spring week with a mean temperature of 10 °C, followed by a week with

mean temperature equal or more than 7–8 °C. Therefore we used this criterion as the onset of spring. During 1998–2010, this indicator week shifted from the 16.5th week to the 14th week of the year defined by the linear regression model (P=0.0172), in the case of the NE counties. However, this shift was not significant in the SW counties, where the indicator week shifted from the 14.2nd week to the 13.6th week of the year (*Fig. 5*).

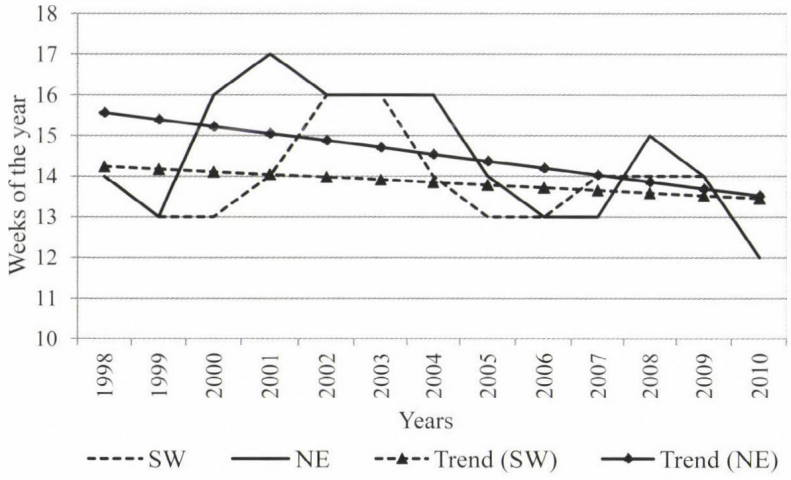

Fig. 5. Shift of the start of the vegetation period based on the temperature> 7–8°C requirement of the questing activity of *Ixodes* ticks in the SW and NE counties in Hungary, in 1998–2010.

3.3. Differences and trends in the regional LB incidences

In periods 1998–2004 and 2005–2010, the percent increase of the cumulative LB incidences showed very heterogenous trends in the different Hungarian counties (*Fig. 6*). In both regions a growing trend could be seen, with P=0.0065 and 0.0471 in the SW and NE counties, respectively. From 1998 to 2010, the trend was consistent in the 3 SW counties, however, no trend could be observed in the 2 NE counties before 2007, and each trend had borderline signficance.

The observations showed that LB incidence rate started to increase rapidly after reaching the weekly rate of 0.1/100.000 from the 16th week and reached the peak period in the 23–25th weeks. Regional differences could be observed in the onset and peak of the LB incidence. In case of the 3 SW counties the weekly LB incidence reached 0.1/100.000 rate in the 11th week and in case of the 2 NE counties, in the 14th week. The LB incidence rate was more than 0.2/100.000 in the SW counties from the 15th week and in the NE counties from the 17th week, the start of LB season showed a 2–3 weeks difference. Aside the above

described slight differences, the shape of the increasing part of the seasons in the two regions were very similar. (*Fig. 7*). The peak of the annual LB curves reached its annual maximum in the 25th week in the SW counties, while in the case of the NE counties, this was observed on the 28th or 29th week, showing a 3-4 weeks difference in the peaks of the LB season by regions. The run of the later summer decreasing part of the LB season showed a more marked 4-5 weeks difference between the SW and NE regions.

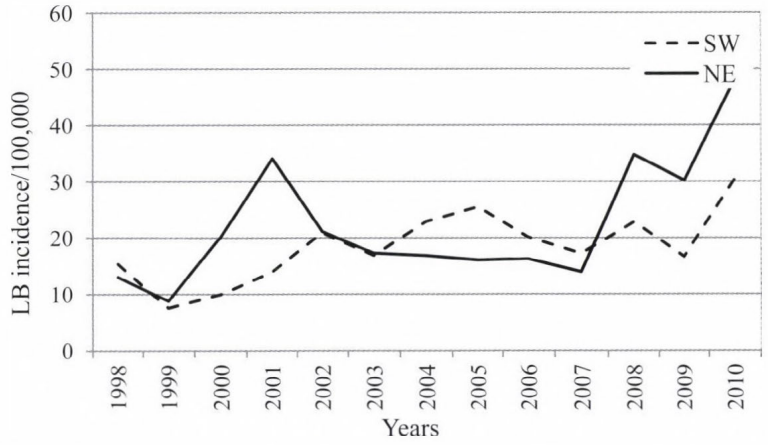

Fig. 6. The annual cumulative LB incidence in the two studied regions (SW and NE), in 1998–2010.

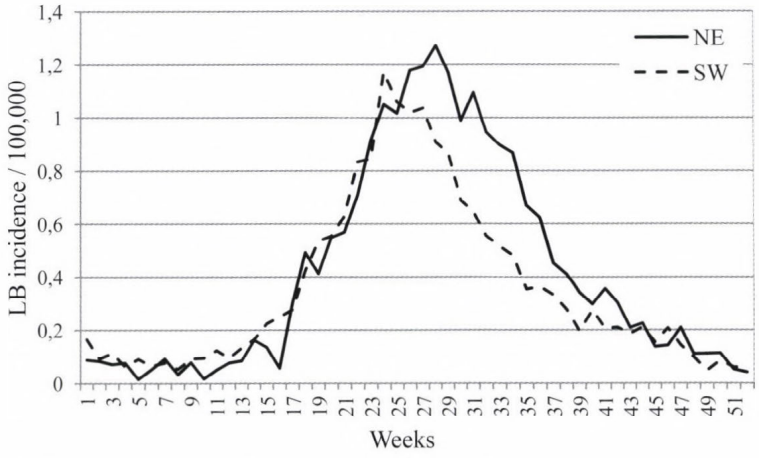

Fig. 7. The average weekly LB incidences of the SW and NE counties in Hungary, in 1998–2010.

While 13 years can not be divided into 2 periods of equal lenght, we compared the periods of 1999–2004 and 2005–2010. Comparing the periods by a polynomial regression model, the peak of the LB season shifted from the 28th to the 29th weeks in the NE counties, while in the SW counties this shift did not reach a one week difference. In the SW counties, the cumulative LB incidence was 118.3/100.000 in period 1998–2003 and 159.18/100.000 in period 2004–2010 (30.55% increase; *Fig. 8*). In the NE counties, the cumulative LB incidence was 92.22 per 100.000 in period 1999–2004 and 132.8/100.000 in period 2005–2010 (25.68% increase; *Fig. 9*).

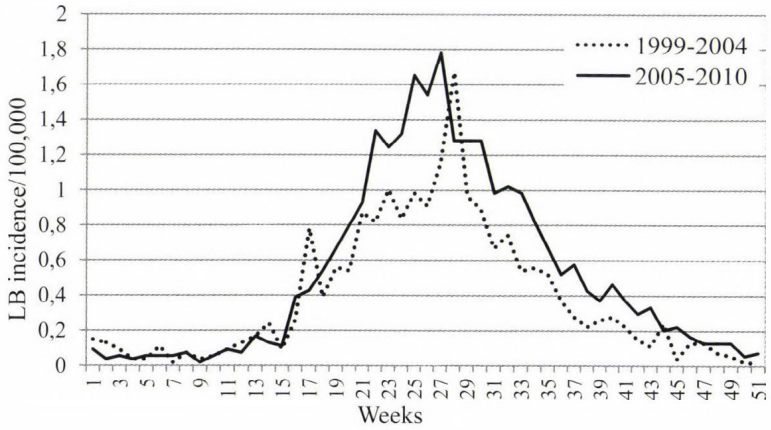

Fig. 8. Average weekly LB incidences of the NE counties in Hungary, in periods 1999–2004 and 2005–2010.

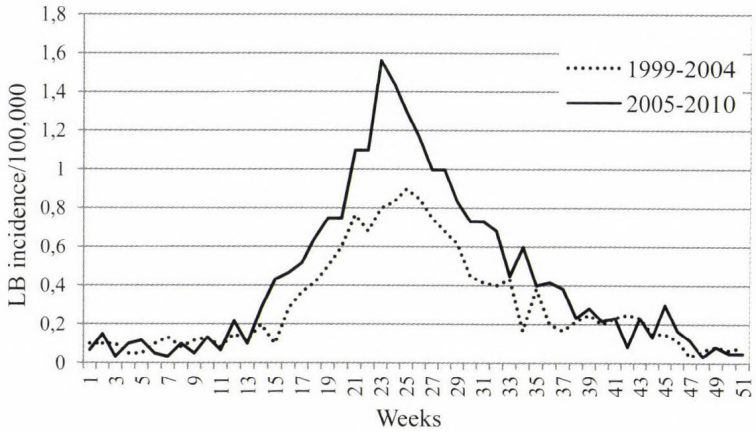

Fig. 9. Average weekly LB incidences of the SW counties in Hungary, in periods 1999–2004 and 2005–2010.

4. Discussion

LB is the most common vector-borne disease in Europe – more common than e.g. the tick-borne encephalitis. Although the disease is not-notificable at the European Community-level, about 85,000 cases are estimated to occur in Europe each year and only in the neighboring country Austria, the annual number of the new LB cases reaches the 14,000–24,000 value (*Lindgren* and *Jaenson*, 2006). With great certainty this amount may be highly underestimated, while it is reported only in few endemic countries. In some countries mainly the complications are reported, not the primary cases with the well recognizable symptom of erythema migrans. The follow-up of the seasonal, monthly, or weekly changes of LB incidence may be more informative than changes in annual incidence with respect to changing climate and the vector, host and pathogen biology. More information can be gained if monthly or weekly changes of the incidence are correlated with meteorological factors.

For routine purposes, temperature is the easiest accessible variable; therefore it seemed to be a first-level aim of the study to investigate whether a relationship between weekly incidence and weekly temperature can be revealed in different climatic regions within a country. This assumption was supported by several studies. LB has been positively correlated with higher summer temperatures in the UK, with a greater number being reported in southwestern regions than in northern areas (*Subak*, 1999).

As a first step, we analyzed the association of temperature and LB at regional level. Although the selected two Hungarian regions have a good contrast concerning the annual mean temperatures mainly in the colder half-year, the sums of annual precipitation of these regions are similar (550–700 mm or more; in period 1970–2000). In the centre of the Hungarian Great Plain, where the annual precipitation sum is the lowest in the Carpathian Basin (550–500 mm or less than 500 mm/year; in period 1970–2000), the annual LB incidences are too low to compare with the wetter Transdanubia region, even in the early summer period. For example, in period 1998–2010 the annual LB incidences in the western part of Transdanubia were 4–10 times higher than in the southern part of the Great Plain. For these reasons we could not make contrast between the wetter and drier Hungarian counties. We observed a 1.6 °C difference in the mean winter temperatures between the northeastern and southwestern regions. Ecologically it may be more important that the mean winter temperature of the NE counties was under 0 °C, while it was above 1 °C in the SW counties. In addition, spring warming started 2 weeks earlier in the SW counties, and there were only 3 weeks of the year in the SW counties, when the weekly mean ambient temperature dropped below 0 °C by a few tenths of a degree. This period lasted for 8 weeks continuously (the main part of the winter) in the NE region.

We did not find a significant correlation between the mean temperature of winter and the following annual LB incidence, which is consistent with

Schauber et al. (2005), who found that the mean temperatures for the prior winter showed weak or inconsistent correlations with Lyme disease incidence. In the period of 1998–2010, LB showed a significant increasing trend in the analyzed NE and SW counties, in the latter region the trend was nearly steadily increasing during the entire period, while in the NE counties this trend was detectable only in the last 4 years. In the colder counties characterized by colder winters, the onset of spring can be detected 1–2 weeks earlier compared to the warmer counties. Although in the analyzed 2 NE counties the onset of spring shifted from the 16.5th week to the 14th week significantly, the peak of the LB season shifted from the 28th to 29th weeks.

Our findings are consistent with *Széll et al.* (2006), who found that *I. ricinus* ticks are most active between April and June. In the 3 SW counties, this indicator week shifted from the 14.2nd to the 13.6th week non-significantly, and the peak of the LB season shifted less than one week. The differences between the onset and the peak of the weekly LB incidence curves can be explained by the regional differences of climate such as the different mean winter and autumn temperatures, since the peak activity of *I. ricinus* is influenced by their local environment (*Hornok* and *Farkas*, 2009).

As described above, in the NE counties the increasing trend of LB incidence started later, but the shifting trend of the spring to the earlier weeks was more rapid than in the SW counties. It remains still open, why a significant shifting trend of the start of spring was not visible in the SW counties, why a slow, but significant increasing trend was observed in the LB incidence rate. It is also at issue what caused the observed 4–5 weeks difference in the decreasing summer part of the LB seasons if the summer precipitation and the temperature conditions were so similar.

On the basis of the results we can conclude, that even a slight difference of 1.6 °C in the mean winter temperatures and 1–2 weeks difference of the start of the vegetation season may influence significantly the features of the LB season.

According to some authors, the monthly mean summer precipitation, the number of summer days with relative humidity more than 85% (*Bennet et al.*, 2006; *Walsh-Haehle*, 2010), or the soil moisture in summer (*Ashley* and *Meentemeyer*, 2004) and the Palmer drought index (*Schauber et al.*, 2005) are as important predictors of LB incidence as the monthly mean summer temperatures.

According to *Bartholy* and *Pongrácz* (2010) and *Schröter et al.* (2005), the total annual precipitation is not expected to change significantly in Hungary, but the seasonal precipitation sums can change by the end of the 21st century. The scenarios showed that summer precipitation would very likely decrease, but the projected precipitation changes would have relatively wide dispersion between 33% and 10%. Based on the seasonal standard deviation values, the largest uncertainty of precipitation change is expected in summer, when LB has the highest incidence values during the year.

Our further aim is to study the expected correlation between the summer precipitation and LB in Hungary, which would be an important additional factor to predict the future of the annual profile of LB incidence in Hungary.

References

Ashley, S.T., Meentemeyer, V., 2004: Climatic analysis of Lyme disease in the United States. *Clim. Res. 27*,177–184.

Bartholy, J. and *Pongrácz, R.,* 2010: Climate change scenarios for the Carpathian Basin. In (Eds. *Faragó, T. et al..*)"VAHAVA" report – Climate change and Hungary: mitigating the hazard and preparing for th impacts Budapest, 12–21.

Bennet, L., Halling, A., and *Berglund, J.*, 2006: Increased incidence of Lyme borreliosis in southern Sweden following mild winters and during warm, humid summers. *Eur. J. Clin. Microbiol. 7,* 426–432.

Brownstein, J.S., Holford, T.R., and *Fish, D.*, 2005: Effect of climate change on Lyme disease risk in North America. *EcoHealth 2*, 38–46.

Confalonieri, U., Menne, B., Akhtar, R., Ebi, K.L., Hauengue, M,, Kovats, R.S.,Revich, B., and *Woodward, A.,* 2007: Human health. In (*Parry et al.* eds.) Climate Change 2007: Impacts, Adaptation and Vulnerability. Contribution of Working Group II to the Fourth Assessment Report of the Intergovernmental Panel on Climate Change, Cambridge University Press, Cambridge, UK, 391–431.

Chauvin, A., Moreau, E., Bonnet, S., Plantard, O., Malandrin, L,. 2009: Babesia and its hosts: adaptation to long-lasting interactions as a way to achieve efficient transmission. Veterinary research, 40(2), 37–37.

Donnelly, A., Jones, MB., and *Sweeney, J.*, 2004: A review of indicators of climate change for use in Ireland. *Int. J. Biometeorol. 49*, 1–12.

Duffy, D.C. and *Campbell, S.R.*, 1994: Ambient air temperature as a predictor of activity of adult Ixodes scapularis (Acari: Ixodidae). *J. Med. Entomol. 31*, 178–180.

English, P.B., Sinclair, A,H,, Ross, Z., Anderson, H., Boothe, V., Davis, C,, Ebi, K., Kagey, B., Malecki, K., Shultz, R., and *Simms, E.*, 2009: Environmental Health Indicators of Climate Change for the United States: Findings from the State Environmental Health Indicator Collaborative. *Environ. Health Perspect. 117*, 1673–1681.

Estrada-Pena, A., 2008: Climate, niche, ticks, and models: what they are and how we should interpret them. *Parasitol. Res. 103*, 87–95.

Földvári, G., Márialigeti, M., Solymosi, N., Lukács, Z., Majoros, G., Kósa, J.P., and *Farkas R.*, 2007. Hard Ticks Infesting Dogs in Hungary and their Infection with *Babesia* and *Borrelia* Species. *Parasitol. Res. 101*, 25–34

Haylock, M.R., Hofstra, N., Klein, A.M.G., Tank, E.J., Klok, P.D., Jones, and *New, M.,* 2008: A European daily high-resolution gridded dataset of surface temperature and precipitation. *J. Geophys. Res. 113*, D20119.

Hornok, S. and *Farkas, R.*, 2009: Influence of biotope on the distribution and peak activity of questing ixodid ticks in Hungary. *Med. Vet. Entomol. 23*, 41–46.

James, N.M., Gage, K.L., and *Khan, A.S.,* 2010: Potential Influence of Climate Change on Vector-Borne and Zoonotic Diseases: A Review and Proposed Research Plan. *Environ. Health Perspect. 118*, 1507–1514.

Kalluri, S., Gilruth, P., Rogers, D., and *Szczur, M.*, 2007: Surveillance of arthropod vector-borne infectious diseases using remote sensing techniques: A review. *PLoS Pathog. 3*, 1361–1371.

Komarek, L., 2005: Magyarország erdősültségének időbeni és területi alakulása. In: (*Puskás J.,* ed.) 4th International Conference on Application of Natural-, Technological and Economical Sciences. Szombathely, Hungary, 28/05/2005 1–6. (in Hungarian)

Kovats, S., Ebi, K., and *Menne, B.*, 2003: Methods of Assessing Human Health Vulnerability and Public Health Adaptation to Climate Change. Health and global environmental change series

No.1 2003 World Health Organization Regional Office for Europe, Copenhagen *KSH*, 2010. január 1. http://portal.ksh.hu/pls/ksh/docs/hun/hnk/Helysegnevkonyv_adattar_2010.xls. Last accessed: 2012.08.02.

Lindgren, E. and *Gustafson, R.*, 2001: Tick-borne encephalitis in Sweden and climate change. *The Lancet. 358,* 16–18.

Lindgren, E. and *Jaenson, T.G.T.*, 2006: Lyme borreliosis in Europe: influences of climate and climate change, epidemiology, ecology and adaptation measures. World Health Organization, Regional Office for Europe, Copenhagen, (http://www.euro.who.int/document/E89522.pdf).

Perret, J.L., Guigoz, E., Rais, O., and *Gern, L.*, 2000: Influence of saturation deficit and temperature on Ixodes ricinus tick questing activity in a Lyme borreliosis-endemic area (Switzerland). *Parasitol. Res. 86*, 554–557.

Randolph, S.E., 2009: Epidemiological consequences of the ecological physiology of ticks. *Adv. Insect Physiol.* 37, 297–339.

Randolph, S.E., 2004: Evidence that climate change has caused 'emergence' of tick-borne diseases in Europe? *Int. J. Med. Microbiol. 293*, 5–15.

Rogers, D.J. and *Randolph, S.E.*, 2006: Climate change and vector-borne diseases. *Adv. Parasitol. 62*, 345–381.

Schauber, E.M., Ostfeld, R.S., and *Evans, A.S. Jr3*, 2005: What is th ebest predictor of annual Lyme disease incidence: Weather, mice or acorns? *Eco. Soc. Am. 2*, 575–586.

Schröter, D., Cramer, W., Leemans, R., Prentice, I.C., Araujo, M.B.; Arnell, N.W., Bondeau, A., Bugmann, H., Carter, T.R., Gracia, C.A., Vega-Leinert, A.C.dl, Erhard, M., Ewert, F., Glendining, M., House, J. I., Kankaanpää, S., Klein, R.J.T., Lavorel, S., Lindner, M., Metzger, M. J., Meyer, J., Mitchell, T.D., Reginster, I., Rounsevell, M., Sabaté, S., Sitch, S., Smith, B., Smith, J., Smith, P., Sykes, M. T., Thonicke, K., Thuiller, W., Tuck, G.;,Zaehle, S., and *Zierl, B.*, 2005: Changes in annual precipitation for the IPCC A2 scenario (2071–2100 compared with 1961–1990) for four different climate models. Ecosystem Service Supply and Vulnerability to Global Change in Europe. Science 310, 13331337.

Széll, Z., Streter-Lancz, Z., Márialigeti, K., and *Streter, T.*, 2006: Temporal distribution of *Ixodes ricinus, Dermacentor reticulatus and Haemaphysalis concinna* in Hungary. *Vet. Parasitol. 141*, 377–379.

Stafford, K.C. III, Cartter, M.L., Magnarelli, L.A., and *Starr-Hope, E., Mshar, P.A.*, 1998: Temporal Correlations between Tick Abundance and Prevalence of Ticks Infected with *Borrelia burgdorferi* and Increasing Incidence of Lyme Disease. *J. Clin. Microbiol. 36*, 1240–1244.

Subak, S,. 1999: Incidence of lyme disease in humans. In: (*Cannell M.G.R. et al.* eds.) Indicators of climate change in the UK. Centre for Ecology and Hydrology, Huntingdon, UK, 38–39.

Tank, K., Wijngaard, A. M. G., Können, J. B., Böhm, G. P., Demarée, R., Gocheva, and *Petrovic, P.*, 2002: Daily dataset of 20th-century surface air temperature and precipitation series for the European Climate Assessment. *Int. J. Climatol. 22*, 1441–1453.

Walsh-Haehle, S., 2010: Vectors, hosts, and the weather: Exploring connections between Lyme disease and climate in the state of Minnesota. *Masters Abstracts Int. 49*, 117.

IDŐJÁRÁS

Quarterly Journal of the Hungarian Meteorological Service
Vol. 117, No. 2, April – June 2013, pp. 187–200

Estimating red noise spectra of climatological time series

István Matyasovszky

Department of Meteorology, Eötvös Loránd University,
Pázmány Péter sétány 1/A, H-1117 Budapest, Hungary
E-mail: matya@caesar.elte.hu

(Manuscript received in final form December 13, 2012)

Abstract–Spectral densities of climatological time series can be generally well approximated by red noise spectra. A common way of the spectral analysis is therefore based on a comparison of the periodogram with a red noise spectrum model. The red noise spectrum is described with the spectral density of a first order autoregressive (AR(1)) model. However, red noise characterized by spectral densities monotone increasing to low frequencies represents a much wider class of processes. The paper provides a concept of estimating red noise spectra without assuming any analytical form of the spectral density. The method, called isotonic regression, is based on robust regression of periodogram elements against frequencies under monotonic constraint of the regression curve. The technique is applied to SOI (Southern Oscillation Index) data from 1866 to 2011, reconstructed NAO (North Atlantic Oscillation) index data from 1659 to 2000, and the Northern Hemisphere temperature proxy data, AD 200–1995. The question of how the isotonic regression performs compared to the traditional AR(1) modeling is discussed.

Key-words: red noise, spectra, autoregressive model, isotonic regression, robust regression

1. Introduction

The task of the spectral analysis is to identify a finite number of discrete frequencies contributing to the discrete spectrum (if exists) and to estimate the spectral density characterizing the continuous spectrum. Spectral densities of climatological time series can be generally well approximated by red noise spectra. A common way of the spectral analysis is therefore to calculate the

periodogram and then to fit a red noise spectrum to model the continuous spectrum. When periodogram exceeds some threshold at a frequency or a range of frequencies, the spectrum is said to differ from the red noise. The threshold depends on the red noise and the significance level selected. The red noise spectrum is generally described with the spectral density

$$f(\lambda)=(\sigma_e^2/\pi)/(1+a^2-2a\cos(\lambda)), \quad \sigma_e^2=\sigma^2(1-a^2) \tag{1}$$

of a first order autoregressive (AR(1)) process with substituting the autoregressive parameter a and variance σ^2 with their consistent estimates $\hat{a}$ and $\hat{\sigma}^2$. This approach is used in such an extent that red noise and AR(1) spectra are seldom used as synonyms. But red noise characterized by spectral densities monotone increasing to low frequencies represents a much wider class of processes than the AR(1) processes.

The purpose of this paper is to provide a general concept of estimating red noise spectra. The method described in Section 2 is based on isotonic regression of the periodogram against frequencies without assuming any analytical form of the spectral density. Isotonic regression includes regression under a monotonic constraint of the regression curve. The technique is applied to SOI data from 1866 to 2011, reconstructed NAO index data from 1659 to 2000, and the Northern Hemisphere temperature proxy data, AD 200–1995 in Section 3. Finally, a section for discussion and conclusions is provided.

2. *Methodology*

2.1. Isotonic regression

Let $x_1,\ldots,x_n$ be a time series observed at $t_1,\ldots,t_n$ as $x_i=g(t_i)+e_i$, where e_i has expectation zero and variance σ^2 for each i, and the sequence $\{e_i\}$ is weakly dependent (*Zhao* and *Woodroofe*, 2012). The task is to provide an estimate $\hat{g}(t)$ for the trend function $g(t)$ under the constraint $\hat{g}(t)\le\hat{g}(s), \quad t<s$. For simplicity, assume that t takes values equidistantly on the interval $[0,1]$. The solution of the least square (LS) problem

$$min\left\{\sum_{k=1}^{n}(x_k-\hat{g}(t_k))^2\right\}, \quad \hat{g}(t_k)\le\hat{g}(t_l), k<l \tag{2}$$

is

$$\hat{g}(t_k) = \max_{i \le k} \min_{k \le j} \frac{x_i + \ldots + x_j}{j - i + 1}$$

for $k = 1,\ldots,n$ and $\hat{g}(t)$ is left-continuous otherwise. The asymptotic behavior of $\hat{g}(t)$ for $t \in (0,1)$ can be written as

$$\hat{g}(t) = g(t) + \frac{2}{n^{1/3}} \left(\frac{1}{2} \sigma^2 g'(t) \right)^{1/3} \cdot \eta, \tag{3}$$

where $g'(t)$ is the derivative of $g(t)$ and η is a random variable following the Chernoff's distribution (*Groeneboom* and *Wellner*, 2001).

Having a time series $y_1,\ldots,y_N$, estimation of the red noise spectra can be performed with the isotonic regression (IR) with substitutions $t = (\pi - \lambda)/\pi$, $x_i = I(\lambda_{n-i+1})$, and $g((\pi - \lambda)/\pi) = f(\lambda)$, where $f(\lambda)$ is the spectral density, and

$$I(\lambda_i) = \frac{1}{\pi N} \left[\left(\sum_{j=1}^{N} y_j \cos(\lambda_i j) \right)^2 + \left(\sum_{j=1}^{N} y_j \sin(\lambda_i j) \right)^2 \right]$$

is the periodogram at frequencies $\lambda_i = (2\pi i)/N, i = 1,\ldots,n$, where n is the largest integer not larger than $N/2$. However, behavior of periodogram elements at frequencies close to the discrete frequencies substantially differs from the behavior of the majority of periodogram elements. Thus, periodogram elements at such frequencies should be taken as outliers, and an IR robust against outliers has to be found. Fortunately, *Álvarez* and *Yohai* (2011) placed the IR in a general framework covering both the ordinary and robust cases. Specifically, note that Eq. (2) is a particular case of

$$\min \left\{ \sum_{k=1}^{n} \rho\left((x_k - \hat{g}(t_k)) / \sigma \right) \right\}, \quad \hat{g}(t_k) \le \hat{g}(t_l), k < l$$

with $\rho(u) = (\sigma u)^2$, and other suitable choices of $\rho(u)$ can deliver robust estimations for $g(t)$. Namely:

$$\hat{g}(t_k) = \max_{u \le k} \min_{k \le v} \{\hat{m}(u,v)\},$$

where $\hat{m}(u,v)$ is the solution of

$$\sum_{j\in C(u,v)} \psi\left((x_i - m)/\sigma\right) = 0 \tag{4}$$

under $C(u,v) = \{j; 1 \le j \le n, u \le t_j \le v\}$, and $\psi(u) = \rho'(u)$. Eq. (3) is then modified by substituting σ^2 with $r\sigma^2$, where

$$r = \frac{E\left[\psi^2(e/\sigma)\right]}{(E[\psi'(e/\sigma)])^2},$$

and e is a random variable that generates $\{e_i\}$. (Note that $r=1$ for Eq. (2).) When estimation of the spectral density $f(\lambda)$ is in question the periodogram $I(\lambda_i)$ is asymptotically $f(\lambda_i)\xi_i$, where ξ_i has standard exponential distribution. Hence σ is not constant but $\sigma_i = f(\lambda_i)$. Therefore, Eq. (4) is modified as

$$\sum_{j\in C(u,v)} \psi\left(x_i / m - 1\right) = 0$$

with $\psi(u)$ based on the function $\psi_H(u) = max\{-c, min\{c,u\}\}$ (*Huber*, 1981) as $\psi(u) = (1-e^{-1})\psi_H(u), u<0$, $\psi(u) = \psi_H(u), u \ge 0$ with choosing $c=1$ (*Matyasovszky*, 2010). The asymptotic behavior of $\hat{f}(\lambda)$ with $\lambda \in (0,\pi)$ is written as

$$\hat{f}(\lambda) = f(\lambda) + \frac{2}{n^{1/3}}\left(-\frac{\pi}{2} f^2(\lambda) f'(\lambda) r\right)^{1/3} \cdot \eta \qquad \text{or}$$

$$f(\lambda) = \hat{f}(\lambda) - \frac{2}{n^{1/3}}\left(-\frac{\pi}{2} f^2(\lambda) f'(\lambda) r\right)^{1/3} \cdot \eta. \tag{5}$$

2.2. Confidence band

In order to detect frequencies where the spectrum differs from red noise, a confidence band for periodogram elements is needed. Therefore, the Chernoff's distribution of η and quantities in Eq. (5) yet unknown should be evaluated. The Chernoff's distribution can be well-approximated by a normal distribution of expectation zero and standard deviation 0.52, but the exact distribution can be found in *Groeneboom* and *Wellner* (2001). The quantity r for the function $\psi(u)$ selected above is $r=0.75$, and the squared spectral density $f^2(\lambda)$ can be substituted by its estimate $\hat{f}^2(\lambda)$. An estimate of $f'(\lambda)$ can be obtained using a

nonparametric regression technique as follows. A data set $y_i = n/(2\pi)\cdot(\hat{f}(\lambda_i) - \hat{f}(\lambda_{i+1}))$, $i = 1,...,n-1$ is constructed as a finite difference approximation to $f'(\lambda_i)$, $i = 1,...,n-1$. The derivative $f'(\lambda)$ is then estimated with the Nadaraya-Watson estimator defined as

$$\hat{f}'(\lambda) = \sum_{j=1}^{n-1} y_j K\left(\frac{\lambda_j - \lambda}{h}\right) \Bigg/ \sum_{j=1}^{n-1} K\left(\frac{\lambda_j - \lambda}{h}\right), \qquad (6)$$

where $K(u)$ is a so-called kernel function and h is the bandwidth. The Epanechnikov kernel is used here that is given by $K(u) = 3/4(1-u^2)$ within [-1, 1] and zero otherwise. The bandwidth having a crucial role in the resulting shape of $\hat{f}'(\lambda)$ can be estimated by minimizing the quantity

$$CV(h) = \sum_{i=1}^{n-1} (y_i - \hat{f}_i'(\lambda_i))^2$$

with respect to h, where $\hat{f}_i'(\lambda_i)$ is calculated by Eq. (6) at $\lambda = \lambda_i$ but with omitting data $y_j, |j-i| \le 1$ from the summation. Note that Eq. (6) is one of the possible solutions of non-parametric curve fitting problems. For further details, see, e.g., *Simonoff* (1996).

The following procedure to give confidence bands for the periodogram is proposed now. 1. Simulate a spectral density $f(\lambda_i)$, $i = 1,...,n$ using Eq. (5). 2. Simulate a periodogram by generating n independent random numbers having exponential distributions with parameters $1/f(\lambda_i)$, $i = 1,...,n$. 3. Repeat steps 1 and 2 10,000 times. 4. Select the $(1-\varepsilon)$th quantile of the simulated periodograms obtained from step 3 at every λ_i. These quantiles provide the critical values for the periodogram calculated from observed data. When periodogram exceeds the critical value determined above at a frequency, the spectrum is said to differ from the red noise at a significance level $(1-\varepsilon)100\%$.

Another basic question is to identify and estimate discrete frequencies. Under general conditions, the limiting probability distribution function of $max_{1\le i\le L}\{\xi_i\} - ln\, n$ is the standard Gumbel distribution function that makes it possible to test the null-hypothesis of lacking discrete frequencies with substituting ξ_i by $I(\lambda_i)/\hat{f}(\lambda_i)$. When the null-hypothesis is rejected at a certain significance level, the second maximum is tested using its asymptotic distribution, and the procedure continues until significant frequencies are

found. Evidently, an existing discrete frequency does not coincide with a detected frequency λ_k, and thus, an improvement of its estimate is needed. A straightforward method is to use the value $\hat{\lambda}_k$ maximizing the periodogram in some neighborhood of λ_k. Consistency and further properties of this technique are discussed in *Chen et al.* (2000).

3. Examples

3.1. Monthly SOI from 1866 to 2011

Monthly values of the Southern Oscillation Index (SOI) are taken from Climate Analysis Section (CAS) of Climate Global Dynamics Division (CGD) at NCAR (http://www.cgd.ucar.edu/cas/catalog/climind/soi.html). The example is chosen intentionally, because SOI does not have red noise but does have colored noise spectrum (e.g., *Chen*, 1982).

The procedure described in Section 2.2 detects three discrete cycles of lengths 12, 6, and 4 months at any reasonable significance level (above the 99.9% significance level). Note that these latter two cycles correspond to integer multiple frequencies of the annual frequency indicating a substantial asymmetry of the annual course. *Fig. 1* demonstrates necessity of the robust IR, because the shape (jumps) of the non-robust isotonic spectral density adapts to discrete cycles, while its robustified version removes the effect of these discrete frequencies. The AR(1) spectral density slightly underestimates the role of high and low frequencies and overestimates the contribution of moderate frequencies (from 4 months to 3.2 years) as compared to the robust isotonic spectral density. However, both techniques recognize a spectral density peak between 2.9-6.5 years (*Fig. 2*). The procedure of *Chen et al.* (2000) to improve the estimation of these cycle lengths results in the highest periodogram value at 6.4 years, but two other local maxima are obtained at 2.9 and 3.5 years. Each of them is significant at the 99% level and is in good agreement with previous several studies (e.g., *Gaucherel*, 2010). The confidence band for the AR(1) spectral density is determined as that for the IR spectral density except for step 1 of Section 2.2. Here the spectral density $f(\lambda_i), i = 1,\ldots,n$ is computed from Eq. (1) with random parameter a that is distributed normally with expectation $\hat{a}$ and variance $(1-\hat{a}^2)/n$ (*Priestley*, 1981).

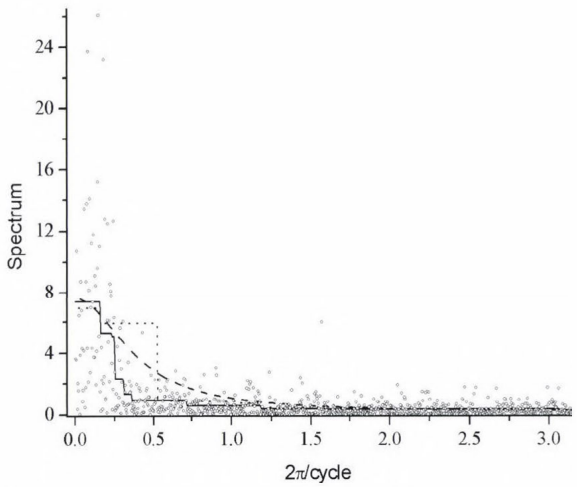

Fig. 1. Periodogram (dot) and spectral density of SOI (1866–2011) estimated by robust isotonic regression (solid), isotonic regression (dotted), and AR(1) model (dashed).

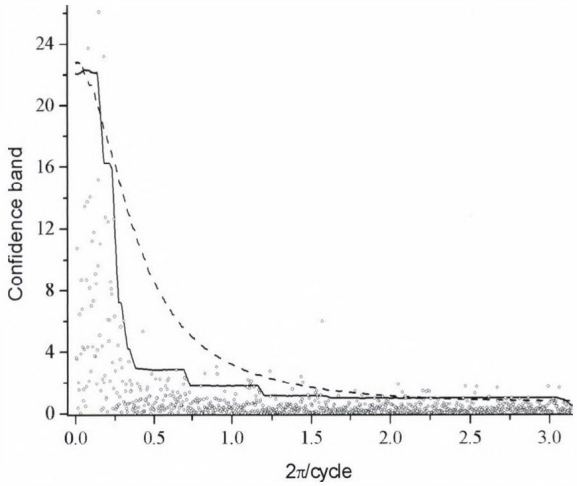

Fig. 2. Upper 95% confidence band of the periodogram (dot) under red noise assumption on the spectral density of SOI (1866–2011) corresponding to the robust isotonic regression (solid) and the AR(1) (dashed) model.

3.2. Reconstructed NAO index from 1659–2000

NAO index values reconstructed by *Luterbacher et al.* (1999; 2002) using instrumental and proxy data from Eurasia are available from 1659 (http://www.esrl.noaa.gov/psd/gcos_wgsp/Timeseries/RNAO/).

A half annual cycle and an annual cycle are detected to be significant at level 91%. The existence of these cycles is ambiguous due to their low significance levels, but an earlier study of *Matyasovszky* (2010) performed with substantially shorter observational data did not find discrete periods at these frequencies. As the contribution of the amplitude of a discrete cycle to the periodogram is proportional to data length and the earlier examination with relatively short data set did not show, but the present study performed with longer data set does show indication for discrete periods at these frequencies, we argue that weak annual and half annul cycles really exist. The third largest periodogram element meets a 65.4-year cycle. This should not be considered as a discrete frequency, but the true spectral density deviates from the red noise spectrum at a 98% significance level corresponding to previous findings. Specifically, dominant 50–70-year periods have been detected in several climatic or climate induced data series (*Loehle* and *Scafetta*, 2011) such as in NAO index (*Mazzarella* and *Scafetta*, 2012). Omitting frequencies close to annual and half annual frequencies a 5.4-year spectral peak significant at a 99% level is notable (*Figs. 3* and *4*) such as in *Box* (2002). Additionally, many other periodogram elements exceed the confidence band at higher frequencies showing the difficulty of detecting deviations from a model spectral density. Namely, assume that the underlying time series has no discrete frequencies and the spectral density is exactly known. Around $\varepsilon \cdot 100\%$ of periodogram elements exceed the $(1-\varepsilon)100\%$ upper confidence band although there are no deviations from the known spectral density at all.

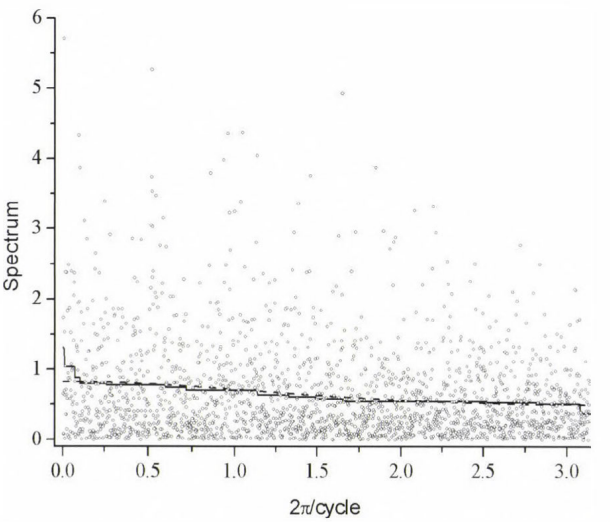

Fig. 3. Periodogram (dot) and spectral density of NAO index (1659–2000) estimated by robust isotonic regression (solid) and AR(1) model (dashed).

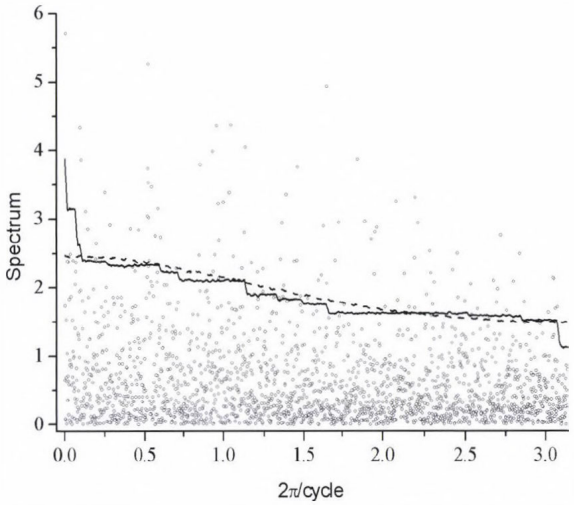

Fig. 4. Upper 95% confidence band of the periodogram (dot) under red noise assumption on the spectral density of NAO index (1659–2000) corresponding to the robust isotonic regression (solid) and the AR(1) (dashed) model.

3.3. Northern Hemisphere temperature from proxy data, AD 200–1995

Annual mean Northern Hemisphere temperatures reconstructed using instrumental and high resolution climate proxy data sources as well as climate modeling studies for the period AD 200–1995 are analyzed. Data are adjusted to the same decadal standard deviation as the instrumental record over the period 1856–1995 (*Jones* and *Mann*, 2004).

As the spectral density is characterized by a sharp peak at low frequencies and a wide flat region at moderate and high frequencies, only cycles longer than 60 years are shown in *Fig. 5*. The AR(1) spectral density seems to be radically overestimated at low frequencies as compared to the IR spectral density. Based on the AR(1) density, the spectrum differs from red noise at cycle lengths around 114, 81, 23, and 11 years at least at the 95% significance level. These cycles are clearly related to the periodicities of solar activity (*Damon* and *Sonett,* 1991). However, the 81-year and 11-year cycles are not reinforced when using the IR spectral density, but further periodicities of 33 and 38 years are detected by both the AR(1) and IR densities (*Fig. 6*). These peaks can be attributed to Atlantic Multidecadal Oscillation (AMO). Although the AMO is generally known as a phenomenon having periodicities 50–70 years (see Section 3.2), other proxy records and model simulations show a more complex structure of periodicities ranging from 30 to 100 years (*Knight et al.*, 2005).

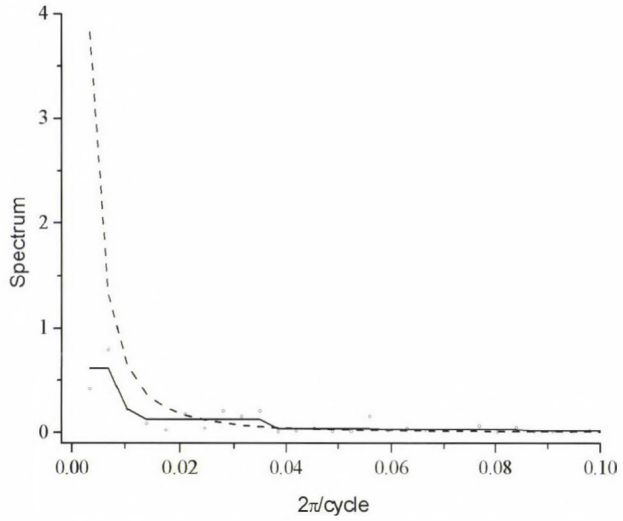

Fig. 5. Periodogram (dot) and spectral density of Northern Hemisphere temperature from proxy data (AD 200-1995) estimated by robust isotonic regression (solid) and AR(1) model (dashed)

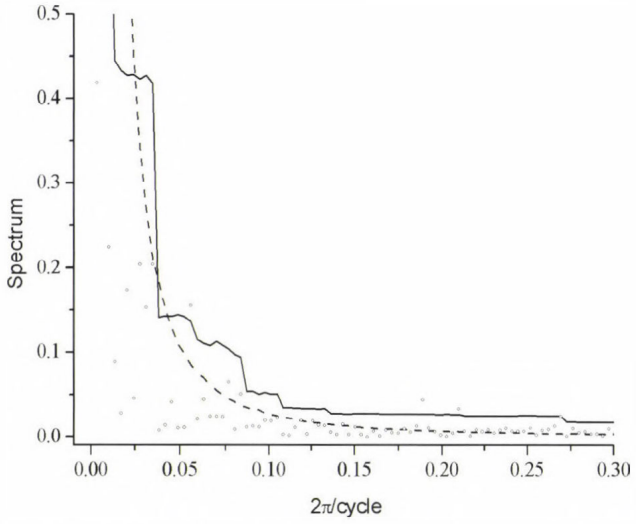

Fig. 6. Upper 95% confidence band of the periodogram (dot) under red noise assumption on the spectral density of Northern Hemisphere temperature from proxy data (AD 200–1995) corresponding to the robust isotonic regression (solid) and AR(1) (dashed) model

4. Discussion

A methodology (robust IR) to estimate red noise spectra has been introduced without any assumption on the analytical form of the spectral density. Although the shape of the spectral densities obtained with the IR method and AR(1) modeling is more or less different (and confidence bands as well), significant deviations from red noise detected with these spectral densities are essentially the same in the first two examples. However, the third example shows important differences between the two approaches. The question of how the proposed IR relates to the traditional AR(1) modeling is addressed now. Suppose we have a general linear stochastic process

$$X_t = \sum_{j=0}^{\infty} b_j e_{t-j} \tag{7}$$

with expectation zero (for simplicity), where e_t has expectation zero and variance σ_e^2, and e_t and e_s are uncorrelated for every $t \neq s$. Note that this class of processes is a very general case in the spectral analysis (e.g., *Priestley*, 1981). It includes MA (moving average) and stationary ARMA (autoregressive-moving average) processes. Additionally, Eq. (7) can be rewritten under general conditions into an infinite AR process and preserving the first p number of autoregressive terms results in an AR(p) representation. The standard AR(1) approximation $X_t^{AR(1)} = a^{AR(1)} X_{t-1}^{AR(1)} + e_t^{AR(1)}$ to Eq. (7) is obtained with $a^{AR(1)} = R(1)$, where $R(1)$ is the one lag autocorrelation. Measuring the accuracy of an AR(1) approximation $X_t^{(a)} = aX_{t-1}^{(a)} + e_t^{(a)}$ to Eq. (7) with $\Delta = E\left[(X_t^{(a)} - X_t)^2\right]$, it can be shown after *Galbraith* and *Zinde-Walsh* (2002) that

$$\Delta = \sum_{j=0}^{\infty} (b_j - (1-a^2)^{1/2} \rho^{1/2} a^j)^2 \sigma_e^2,$$

where $\rho = \sum_{j=0}^{\infty} b_j^2$. In other words, the best AR(1) model is achieved with a that minimizes Δ, which, however, differs from $R(1)$. Hence, an AR(1) process with autoregressive coefficient $a^{AR(1)} = R(1)$ is not the best approximating model in the mean squared error sense.

Forgetting about this fact and just focusing on the question of how the spectral density of X_t is approximated with the spectral density of $X_t^{AR(1)}$, the following details can be provided. It is known that the spectral density Eq. (1) of an AR(1) process is consistently estimated when parameters a and σ_e^2 are

substituted with their consistent estimates (*Mann* and *Wald*, 1943), but it is unrealistic that a time series comes from an AR(1) process. The spectral density of a linear process is consistently estimated by the spectral density of an AR(p) process when $p \to \infty, p^3 / n \to 0$ as $n \to \infty$ (*Berk*, 1974). However, fixing the value $p = 1$, nothing is known about the accuracy of such an estimate without knowing the true spectral density. Additionally, these results hold only for purely continuous spectra. For this latter reason, *Mann* and *Lee* (1996) proposed to fit AR(1) spectra to median smoothed periodogram elements. This is because median is robust against outliers of the periodogram, which might be present due to potentially existing discrete frequencies. But neither this approach quits the analytical form Eq. (1) of the spectral density, and hence we do not really know what the spectral density of the traditionally fitted AR(1) model represents. In contrast, the IR is a technique without any assumption on the analytical form of the spectral density. It is based on the least square (LS) estimation which is not too efficient for random variables far from Gaussian. However, the LS IR is identical with the maximum likelihood (ML) IR in some specific situations. This is the case for exponential distributions, and hence the LS IR represents the ML estimate of the spectral density under monotone decreasing constraint, because the periodogram elements have asymptotical exponential distributions.

A generalized method of IR (*Tibshirani et al.*, 2011), the so-called nearly-isotonic regression (NIR), permits the possibility of deviations from monotonicity when necessary. The necessity of monotonicity violations is controlled via a parameter that is estimated within the procedure. Adapting this technique to periodograms makes it possible to detect departures from red noise. Applying the NIR to SOI data clearly shows a local maximum of the spectral density between cycles of 3.4–7.5 years (*Fig. 7*). As the NIR is not a robust technique, the previously detected discrete frequencies were omitted. This may be done because the NIR can handle unevenly spaced data as well. *Fig. 8* shows the spectral density obtained with the NIR for NAO index time series. It can be concluded that annual and half annual cycles form a discrete spectrum, because so sharp spectral peaks should be due to discrete spectra. Additionally, the NIR spectrum is somewhat higher at low frequencies than the robust IR spectrum indicating that the 65.4-year cycle is an outlier in the robust IR, and hence the spectrum strongly deviates here from the red noise spectrum. The difference between spectral densities obtained with the robust IR and NIR is negligible for the third example (Northern Hemisphere temperature from proxy data, AD 200-1995). As the NIR makes it possible to detect departures from red noise, it seems that estimating red noise spectra either with AR(1) modeling or IR is unnecessary. Unfortunately, statistical properties of the NIR technique are not available, and hence the accuracy of this procedure is not known. Therefore, usage of the methodology based on the IR is advised as described in the paper.

Acknowledgement-The European Union and the European Social Fund provided financial support for the project under the grant agreement no. TÁMOP 4.2.1./B-09/KMR-2010-0003.

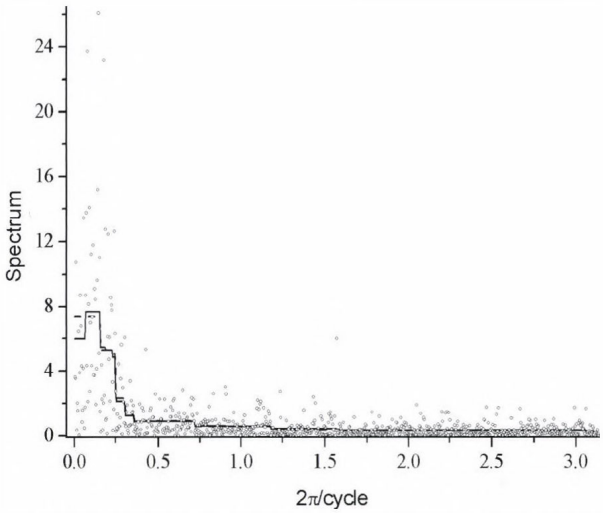

Fig. 7. Periodogram (dot) and spectral density of SOI (1866–2011) estimated by nearly isotonic regression (solid) and robust isotonic regression (dashed)

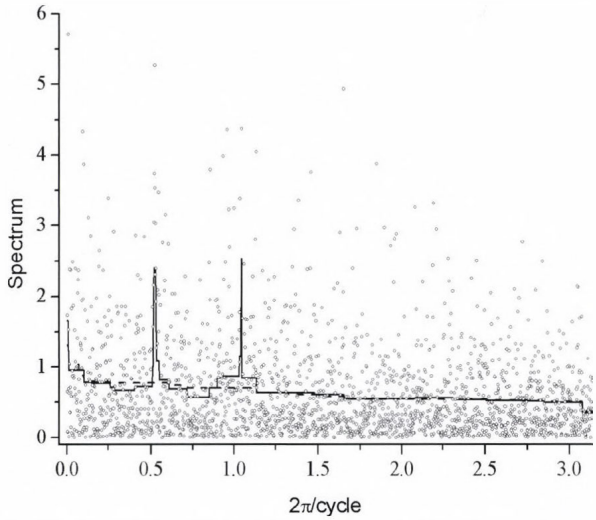

Fig. 8. Periodogram (dot) and spectral density of NAO index (1659-2000) estimated by nearly isotonic regression (solid) and robust isotonic regression (dashed)

References

Álvarez, E.E. and *Yohai, V.J.*, 2011: M-estimators for Isotonic Regression. arXiv: 1105.5065v1[stat.ME]

Berk, K.N., 1974: Consistent autoregressive spectral estimates. *Ann. Math. Stat. 2*, 489–502.

Box, J.E., 2002: Survey of Greenland instrumental temperature records: 1873–2001. *Int. J. Climatol. 22*, 1829–1847.

Chen, W.Y., 1982: Assessment of Southern Oscillation sea-level pressure indices. *Mon. Weather Rev. 113*, 1876–1888.

Chen, Z.G., Wu, K.H. and *Dahlhaus, R.*, 2000: Hidden frequency estimation with data tapers. *J. Time Ser. Anal. 21*, 113–142.

Damon. P.E. and Sonnett, C.P., 1991: Solar and terrestrial components of the atmospheric ^{14}C variation spectrum. In (Eds: *Sonnett, C.P., et al.*) The Sun in Time. University of Arizona Press, Tucson.

Galbraith, J.V. and *Zinde-Walsh, V.*, 2002: Autoregressive Approximation, with Econometric Applications, 401–421. In (Eds: *Ullah, A., et al.)* A Handbook of Applied Econometrics and Statistical Inference. Marcel Dekker, New York.

Gaucherel, C., 2010: Analysis of ENSO interannual oscillations using non-stationary quasi-periodic statistics: a study of ENSO memory. *Int. J. Climatol. 30*, 926–934.

Groeneboom, P. and *Wellner, J.A.*, 2001: Computing Chernoff's Distribution. *J. Comput. Graph. Stat. 10*, 388–400.

Huber, P.J., 1981: Robust statistics. Wiley, New York

Jones, P. D. and Mann, M.E., 2004: Climate over past millennia. *Rev. Geophys. 42*, RG2002.

Loehle, C. and *Scafetta, N.*, 2011: Climate Change Attribution Using Empirical Decomposition of Climatic Data. *Open Atm. Sci. J. 5*, 74–86.

Knight, J.R., Allan, R.J., Folland, C.K., Vellinga, M. and *Mann, M.E.*, 2005: A signature of persistent natural thermohaline circulation cycles in observed climate. *Geophys. Res. Lett. 32*, L20708.

Luterbacher, J., Schmutz, C., Gyalistras, D., Xoplaki, E. and *Wanner, H.*, 1999: Reconstruction of monthly NAO and EU indices back to AD 1675. *Geophys. Res. Lett. 26*, 2745–2748.

Luterbacher, J., Xoplaki, E., Dietrich, D., Jones, P.D., Davies, T.D., Portis, D., Gonzalez-Rouco, J.F., von Storch, H., Gyalistras, D., Casty, C. and *Wanner, H.*, 2002: Extending North Atlantic Oscillation Reconstructions Back to 1500. *Atmos. Sci. Lett.*, doi:10.1006/asle.2001.0044.

Mann, H.B. and *Wald, A.*, 1943: On the statistical treatment of stochastic difference equations. *Econometrica 11*, 173–220.

Mann, M.E. and *Lee, J.M.*, 1996: Robust estimation of background noise and signal detection in climatic time series. *Climatic Change 33*, 409–445.

Matyasovszky, I., 2010: Improving the methodology for spectral analysis of climatic time series. *Theor. Appl. Climatol. 101*, 281–287.

Mazzarella, A. and *Scafetta, N.*, 2012: Evidences for a quasi 60-year North Atlantic Oscillation since 1700 and its meaning for global climate change. *Theor. Appl. Climatol. 107*, 599-609.

Priestley, M.B., 1981: Spectral Analysis and Time Series. Academic Press, New York.

Simonoff, J.S., 1996: Smoothing Methods in Statistics. Springer Series in Statistics, Springer-Verlag, New York.

Tibshirani, R.J., Hoefling, H. and *Tibshirani, R.*, 2011: Nearly-Isotonic Regression. *Technometrics 53*, 54–61.

Zhao, O. and *Woodroofe, M.*, 2012: Estimating a monotone trend. *Stat. Sinica 22*, 359–378.

IDŐJÁRÁS

Quarterly Journal of the Hungarian Meteorological Service
Vol. 117, No. 2, April – June 2013, pp. 201–218

An IMEX scheme combined with Richardson extrapolation methods for some reaction-diffusion equations

István Faragó[1,2*], Ferenc Izsák[1], and Tamás Szabó[3,4]

[1] *Department of Applied Analysis and Computational Mathematics*
Eötvös Loránd University
H-1117, Budapest, Pázmány P. sétány 1/c. Hungary

[2] *HAS-ELTE Reserch Group "Numerical Analysis and Large Networks"*
H-1117, Budapest, Pázmány P. sétány 1/c. Hungary

[3] *BCAM Basque Center for Applied Mathematics*
Alameda Mazarredo, 14, E - 48009 Bilbao
Basque Country, Spain

[4] *CAE Engineering Kft.*
H-1122, Budapest, Ráth György u. 28. Hungary

e-mails: faragois@cs.elte.hu, izsakf@cs.elte.hu, szabot@cs.elte.hu

**Corresponding author*

(Manuscript received in final form March 3, 2013)

Abstract–An implicit-explicit (IMEX) method is combined with some so-called Richardson extrapolation (RiEx) methods for the numerical solution of reaction-diffusion equations with pure Neumann boundary conditions. The results are applied to a model for determining the overpotential in a Proton Exchange Membrane (PEM) fuel cell.

Key-words: IMEX, reaction-diffusion equations, Richardson extrapolation, fuel cell, PEM, numerical solution

1. Introduction

The numerical solution of advection-reaction-diffusion equations is a central problem in the numerical analysis. In practice, many important meteorological phenomena are modeled using reaction-diffusion equations (which are often supplemented with advection terms). Therefore, the efficient numerical solution of these equations is of central importance. The numerical treatment of the boundary layer effect and the possibly stiff terms lead to challenging problems. The importance of this topic lies in the applicability of the corresponding models in the natural sciences including atmospheric modeling.

A previously (*Faragó et al.*, 2013) presented implicit-explicit (IMEX) method of second order in space is supplemented with Richardson extrapolation methods (passive and active) in time. The new method is developed for the numerical solution of reaction-diffusion equations with pure Neumann boundary conditions in order to have a method of second order both in space and time. Richardson extrapolation is a very efficient method to increase the accuracy of many numerical methods. It consists of applying a given numerical scheme with different discretization parameters (in our case different time steps) and combining the obtained results with properly chosen weights (*Zlatev et al.*, 2010).

2. Motivation

The method which we start from is stable under very mild conditions. If we can enhance also its time accuracy, we can have an efficient algorithm. In the atmospheric modeling it is particularly useful, since a fast method leading to an up-to-date forecast needs relatively large time steps. At the same time, in real life situations we have to run the corresponding simulations over many time steps, so the stability of the method is of primary importance.

To get a complex one-dimensional reaction-diffusion problem we cite here an interesting electrochemical model. Nowadays, electrical energy is the cleanest and most versatile energy that can be used in almost all fields of life. Due to the technical improvements, the utilization and efficiency of producing electrical energy are increasingly growing.

In this section, we compute numerically the overpotential in PEM fuel cells. These kinds of fuel cells "burn" hydrogen fuel and oxygen to water, producing electrical energy at a high efficiency without air pollution. Their operation can be reversible: they can also convert electrical energy into chemical energy.

The electro-chemical reactions take place at the anode and cathode on the boundary of two phases (solid and solution phase), while the charge neutrality is macroscopically preserved.

Complex models (*Ziegler et al.*, 2005) are needed to solve different phenomenological equations such as the Nernst-Planck equation for multiple mass transport, the Stefan-Maxwell equation for heat transfer, Ohm's law for ionic migration and electron conductivity, and the equations of electrochemical kinetics. These models are usually solved by using only a single solver, e.g., Runge-Kutta, Newton, or Crank-Nicholson methods.

Subramanian et al. (2007) developed a method to reduce the number of the governing equations of Li-ion battery simulation by using different mathematical techniques. The original problem with a proper discretization has 4800 equations which can be reduced to 49, and finally, the simulation time of the discharge curve can be cut to 85 ms. However, in this model the double-layer capacitance was not included.

We focus here only on the evolution of the overpotential and we take into consideration both the inhomogeneity of the conducting media and the presence of the different phases in the cell. We perform the computations with realistic parameters.

2.1. Physical laws: homogeneous and heterogeneous models

In practice, a consumer (some kind of electric device) is inserted into an electrical circuit, which is feeded by the fuel cell. We assume that the current in the outer circuit is known ($I(t)$) and we can control it. The aim of the following investigation is to calculate the corresponding voltage, which is called the cell potential. This gives also the electric energy provided by the fuel cell, which is very important in the course of evaluating the performance of a fuel cell.

According to Kirchoff's law, the cell potential E_{cell} can be calculated by the following equation, see also *Litster* and *Djilali*, (2007):

$$E_{cell}(t) = E_{OC}(t) - \eta^a(t) - \frac{W_{mem}}{\kappa_{mem}} I(t) - V^*(t), \tag{1}$$

where $t \in (0,T)$ denotes time. Here $E_{OC}(t) \approx 1.23\text{V}$ denotes the open circuit potential, which is present between the anode and cathode without the presence of any consumer.

Considering the simplest form of Ohm's law, the term $\frac{W_{mem}}{\kappa_{mem}} I(t)$ means the potential loss at the membrane, the thickness and conductivity of which are denoted by W_{mem} and κ_{mem}, respectively.

The calculation of the last quantity on the right-hand side (V^*), which refers to the potential loss at the cathode, needs a detailed analysis. The interval $(0, L)$ refers to the thickness of the cathode, where two phases are distinguished:

- The solution phase, where the hydrogen ions are conducted according to the rate κ_{eff}. The potential and the current density in this phase are denoted by ϕ_2 and i_2, respectively.
- In the solid phase of the cathode, electrons are conducted according to the rate σ_{eff}. The potential and the current density here are denoted by ϕ_1 and i_1, respectively.

All of these quantities could be allowed to depend on time and space corresponding to the given assumptions and the structure of the fuel cell and the time evolution of the process.

Using the defined quantities, V^* in Eq. (1) can be given as

$$V^*(t) = \phi_1(t, L) - \phi_2(t, 0), t \in (0, T). \tag{2}$$

The quantity we investigate in the governing equations is the overpotential

$$\eta(t, x) = \phi_1(t, x) - \phi_2(t, x) \geq 0, x \in (0, L), t \in (0, T). \tag{3}$$

In the calculation of the potentials, we choose the reference level to be at the left end of the solution phase, i.e., we define $\phi_2(t, 0) = 0$. This is in a good accordance with the uniqueness of the solutions in the corresponding equations. As we will see, the governing equations depend only on the spatial derivatives of the potentials, such that the above assumption is necessary to determine both $\phi_2(t, x)$ and $\eta_2(t, x)$. Then an immediate consequence of (2) and (3) is that

$$V^*(t) = \phi_1(t, L) = \eta(t, L) + \phi_2(t, L). \tag{4}$$

Applying Ohm's law for both phases we obtain

$$\begin{aligned} i_1(t, x) &= -\sigma_{eff}(x)\partial_x\phi_1(t, x) \\ i_2(t, x) &= -\kappa_{eff}(x)\partial_x\phi_2(t, x) \end{aligned} \tag{5}$$

and the principle of electroneutrality gives

$$-\partial_x i_1(t, x) = \partial_x i_2(t, x). \tag{6}$$

The conservation law for the currents (see *Newman* and *Thomas-Alyea*, 2004) results in the formula

$$\partial_x \left(\kappa_{eff}(x)\partial_x \phi_2(t,x)\right) = \\ -a(x)C_{dl}(x)\partial_t \eta(t,x) - a(x)i_0(x)g\left(\alpha \frac{F}{RT}\eta(t,x)\right). \tag{7}$$

Here, the function $C_{dl}(x)$ gives the double-layer capacitance at the cathode side, and the last term yields the faradic current with $i_0(x)$, the exchange current density at the cathode. For the notations of the material coefficients we refer to the Appendix. The function $g : \mathbb{R} \to \mathbb{R}$ refers to the kinetics of the oxygen reduction reaction here. This should be an increasing function with $g(0) = 0$.

Remark 2.1: *Among the several approaches for the sake of simplicity we apply linear kinetics and, accordingly, we use*

$$g_L(u) = c(x)u, \tag{8}$$

where $c(x)$ *is a given bounded non-negative function. Other possible choices are the following, which are going to be used in the course of the analysis and the numerical experiments* (*Kriston et al.*, 2010).

- *Butler–Volmer kinetics*:

$$g_{BV}(u) = c(x)(\exp(u) - \exp(-u)), \tag{9}$$

- *diffusion kinetics*:

$$g_D(u) = j_D(x)\left(\frac{c(x)\exp(u)}{c(x)(\exp(u)+j_D(x)} - \frac{c(x)\exp(-u)}{c(x)\exp(-u)+j_D(x)}\right), \tag{10}$$

where $j_D(x)$ *is the limiting current, which in this equation is acting as a diffusion coefficient. This choice provides the most accurate model of the cathode reaction.*
In what follows the notation $g(u)$ *stands for any of the above functions* (g_L, g_{BV}, g_D).

At the left end of the cathode, only the protons can exit to the membrane and similarly, at the right end (at the current collector), only the electrons can

leave the cathode. Therefore, $\partial_x \phi_1(t,0) = 0$ and $\partial_x \phi_2(t,L) = 0$ such that using Eq. (3) we have the following boundary conditions:

$$\partial_x \eta(t,0) = -\partial_x \phi_2(t,0) = -\frac{1}{\kappa_{eff}(0)} I(t),\ t \in (0, t_{max}),$$
$$\partial_x \eta(t,L) = \partial_x \phi_1(t,L) = \frac{1}{\sigma_{eff}(L)} I(t),\ t \in (0, t_{max}). \tag{11}$$

Although we have listed all physical principles and the governing equations here, the corresponding equations are not yet ready for the solution, since Eq. (7) contains also the unknown term $\phi_2(t,x)$.

2.2. Governing equations in the heterogeneous case

In this section we will obtain an explicit equation for the overpotential $\eta(t,x)$ by eliminating the term $\phi_2(t,x)$ in Eq. (7) without assuming constant material and kinetic coefficients.

The physical laws in Eqs. (5), (6), (7), and (11) can be rewritten into a single reaction-diffusion equation of type Eq. (21) for the unknown function η:

$$aC_{dl}\partial_t \eta(t,x) = \partial_x \left(\frac{\kappa_{eff}}{\kappa_{eff}+\sigma_{eff}}\right)\left(-I(t) + \sigma_{eff}\partial_x \eta(t,x)\right)$$
$$+ \frac{\kappa_{eff}}{\kappa_{eff}+\sigma_{eff}} \partial_x \left(\sigma_{eff}\partial_x \eta(t,x)\right) - ai_0 g\left(\alpha \frac{F}{RT}\eta(t,x)\right)$$
$$= \partial_x \left[\frac{\kappa_{eff}\sigma_{eff}}{\kappa_{eff}+\sigma_{eff}} \partial_x \eta(t,x)\right] - \partial_x \left(\frac{\kappa_{eff}}{\kappa_{eff}+\sigma_{eff}}\right) I(t)$$
$$-ai_0 g\left(\alpha \frac{F}{RT}\eta(t,x)\right) \tag{12}$$

For the corresponding initial-boundary value problem we use the initial value

$$\eta(0,x) = 0,\ x \in (0,L), \tag{13}$$

and (12) is equipped with the Neumann type boundary conditions in Eq. (11).

Remark: We can express $\phi_2(t,x)$ as

$$\partial_x \phi_2(t,x) = \frac{1}{\kappa_{eff}(x)+\sigma_{eff}(x)}\Big(I(t) - \sigma_{eff}(x)\partial_x\,\eta(t,x)\Big), \tag{14}$$

and consequently, by the assumption $\phi_2(t,0) = 0$ (see the explanation after Eq. (3)) we have

$$\phi_2(t,x) = \int_0^x \left(-\frac{\sigma_{eff}(t,s)}{\kappa_{eff}(t,s)+\sigma_{eff}(t,s)}\partial_s\eta(t,s) + \frac{1}{\kappa_{eff}(t,s)+\sigma_{eff}(t,s)}I(t)\right) ds. \tag{15}$$

Therefore, according to (4) we can give the potential loss V^* at the anode as

$$V^*(t) = \eta(t,L) + \phi_2(t,L)$$
$$= \eta(t,L) + \int_0^L -\frac{\sigma_{eff}(t,s)}{\kappa_{eff}(t,s)+\sigma_{eff}(t,s)}\partial_s\eta(t,s) + \frac{1}{\kappa_{eff}(t,s)+\sigma_{eff}(t,s)}I(t)\,ds. \tag{16}$$

This completes the computation of the right-hand side of Eq. (1), and the desired quantity $E_{cell}(t)$ can be given.

Remark: According to the notations of the second section of this work, we have that

$$p = \frac{1}{aC_{dl}}, \quad q = \frac{\kappa_{eff}\sigma_{eff}}{\kappa_{eff}+\sigma_{eff}}, \quad \text{and}$$

$$F\big(t,x,\eta(t,x)\big) = -\frac{i_0}{C_{dl}}\,g\left(\alpha\frac{F}{RT}\eta(t,x)\right) - \frac{1}{aC_{dl}}\partial_x\left(\frac{\kappa_{eff}}{\kappa_{eff}+\sigma_{eff}}\right)I(t). \tag{17}$$

2.3. Model problem

For testing the method in the article, we investigate here a model problem. Based on real measurements we have
$\kappa_{eff} \approx 0.002$ and $\sigma_{eff} \approx 1.8$, and accordingly, we define

$$\kappa_{eff}(t,x) \approx 0.002 - 0.001x \text{ and } \sigma_{eff}(t,x) \approx 1.8 + 0.001x. \tag{18}$$

Consequently,

$$\kappa_{eff} + \sigma_{eff} = 1.801 \quad \text{and} \quad \frac{\kappa_{eff}}{\sigma_{eff}+\kappa_{eff}}(t,x) = \frac{2-x}{1801} \ .$$

For simplicity, we did not incorporate time dependence yet, but our analysis extends also to the case of time dependent conductivity parameters. If the analytic solution of the governing equation Eq. (12) is

$$\eta(t,x) = \frac{t^2}{4} \cdot \left(1 + (x - \frac{1801}{1803})^2\right), \tag{19}$$

we can verify that the equalities

$$\begin{aligned} -\frac{1}{\kappa_{eff}(t,0)} I(t) &= \partial_x \eta(t,0) = \frac{t^2}{2}\frac{1801}{1803} \ , \\ \frac{1}{\sigma_{eff}(t,1)} I(t) &= \partial_x \eta(t,1) = -\frac{t^2}{2}\left(1 - \frac{1801}{1803}\right) \end{aligned} \tag{20}$$

hold true such that $\partial_x \eta(t,0)$ and $\partial_x \eta(t,1)$ correspond to u_l and u_r in Eq. (12), where $I(t) = 10^{-3} \cdot \frac{1801}{1803} t^2$. These show that the boundary conditions in Eq. (11) are satisfied.
Using all parameters we can give $C_{dl}(x)$ such that η in Eq. (19) is the solution of Eq. (12) with the boundary conditions in Eq. (11).

It is justified to use the numerical method in Section 4 to approximate u, since the Assumptions 1, 2, and 3 are satisfied:

- According to (17) and the choice of the linear kinetics,

$$\partial_3 F(t,x,u) = c(x)\alpha \frac{F}{RT},$$

which is bounded.

- The coefficient functions p and q given in Eq. (17) are obviously positive.
- The inequalities in Assumption 3 have been verified consecutively in the time steps during the simulations. These results are shown in *Fig. 1*. One can see that using a reasonably accurate space discretization, we can simulate the underlying process over sufficiently long time.

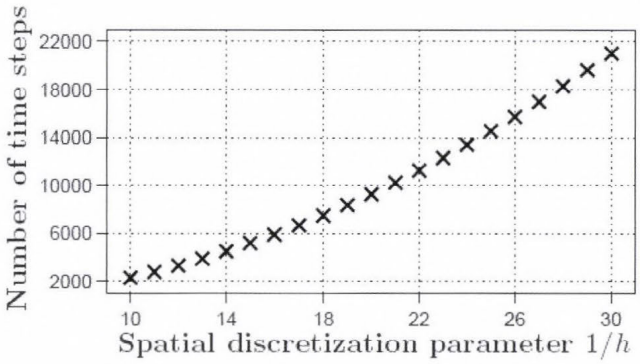

Fig. 1. Number of steps N with step length $\tau = 1$ s until Assumption 3 is satisfied vs. the number n of the grid points on the interval $I = 1$ cm.

3. Finite difference approximation

We use the following reaction-diffusion equation as a prototype to investigate some finite difference approximation:

$$\begin{cases} \partial_t u(t,x) = p(t,x)\partial_x\big(q(t,x)\partial_x u(t,x)\big) + F\big(t,x,u(t,x)\big), t \in (0,T), \quad x \in I \\ u(0,x) = u_0(x), \quad x \in I \\ \partial_x u(t,h_l) = u_l(t),\ \partial_x u(t,h_r) = u_r(t), \quad t \in (0,T), \end{cases} \tag{21}$$

for the unknown function u on the interval $I = (h_l, h_r) \subset \mathbb{R}$ over the time domain $[0,T)$, where the coefficient functions $p, q \in C^1([0,T] \times I)$, the reaction term $F \in C^1([0,T] \times I \times \mathbb{R})$, and the fluxes $u_l, u_r \in C^1[0,T]$ are given.

For the numerical approximation we use a staggered grid: I is divided into n uniform subintervals of length
$h = \frac{h_r - h_l}{n}$ such that

$$h_j := h_l + \frac{2j-1}{2|I|}, j = 1,2,\dots,n \text{ and } h_{j+\frac{1}{2}} := h_l + \frac{j}{|I|}, j = 0,1,\dots,n$$

denote the midpoints and the endpoints of the subintervals, respectively, as shown in the following figure:

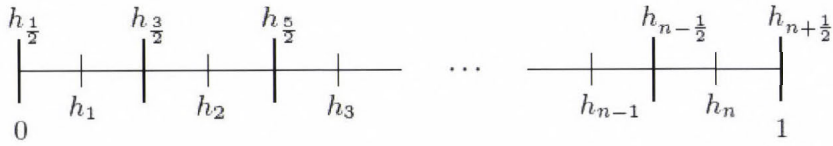

For the time discretization we use the time step $\tau = \frac{T}{N}$ and the notation $t_k := \tau \cdot k$.

We denote the vector of unknowns by

$$\boldsymbol{u}^k = (u_1^k, u_2^k, \dots, u_n^k),$$

where $u_j^k \approx u(t_k, h_j)$. The values of the coefficient function $p_j^k = p(t_k, h_j)$ are defined in the midpoints of the subintervals, i. e., $k = 0,1, \dots, N$ and $j = 1,2, \dots, n$. Accordingly, we use the notations

$$\boldsymbol{u}(k,\cdot) = (u(t_k, h_1), u(t_k, h_2), \dots, u(t_k, h_n))^T \quad ,$$

and

$$\boldsymbol{F}(t_{k+1}, h, \boldsymbol{u}^k) = (F(t_{k+1}, h_1, u_1^k), \dots, F(t_{k+1}, h_n, u_n^k))^T.$$

At the same time, the values of the coefficient function $q_{j+\frac{1}{2}}^k = q\left(t_k, h_{j+\frac{1}{2}}\right)$ are computed at the end points of the subintervals, i. e., $k = 0,1, \dots, N$ and $j = 0,1, \dots, n$.

4. The IMEX scheme

We developed a finite difference scheme reported in *Faragó et al.*, (2013). To discuss the corresponding extrapolation method, we summarize the notations and results in *Faragó et al.*, (2013). For the proof of the statements we refer to this work. We developed a finite difference scheme following the *method of lines*: the vector of unknowns at the $(k + 1)$th time step is determined from that at the kth time step (*Faragó et al.*, 2013).

Using the notations in Section 3, we consider the following finite difference approximation of Eq. (21):

$$
\begin{cases}
u_j^0 = u_0(h_j),\ j = 1,2,3,\dots,n \\
\frac{u_j^{k+1}-u_j^k}{\tau} = \frac{1}{h}p_j^{k+1}\left(q_{j+\frac{1}{2}}^{k+1}\frac{u_{j+1}^{k+1}-u_j^{k+1}}{h} - q_{j-\frac{1}{2}}^{k+1}\frac{u_j^{k+1}-u_{j-1}^{k+1}}{h}\right) \\
+F\left(t_{k+1}, h_j, u_j^k\right),\ k = 0,1,\dots,N-1, j = 2,3,\dots,n-1 \\
\frac{u_1^{k+1}-u_1^k}{\tau} = \frac{1}{h}p_1^{k+1}\left(q_{\frac{3}{2}}^{k+1}\left(\frac{u_2^{k+1}-u_1^{k+1}}{h} + \frac{\frac{3}{23}u_2^{k+1}-\frac{2}{23}u_1^{k+1}-\frac{1}{23}u_3^{k+1}}{h} - \frac{1}{23}u_l(t_{k+1})\right)\right. \\
\left. - q_{\frac{1}{2}}^{k+1}u_l(t_{k+1})\right) + F\left(t_{k+1}, h_1, u_1^k\right),\ k = 0,1,\dots,N-1 \\
\frac{u_n^{k+1}-u_n^k}{\tau} = \frac{1}{h}p_n^{k+1}\left(-q_{n-\frac{1}{2}}^{k+1}\left(\frac{u_n^{k+1}-u_{n-1}^{k+1}}{h} - \frac{\frac{3}{23}u_{n-1}^{k+1}-\frac{1}{23}u_{n-2}^{k+1}-\frac{2}{23}u_n^{k+1}}{h} - \frac{1}{23}u_r(t_{k+1})\right)\right. \\
\left. + q_{n+\frac{1}{2}}^{k+1}u_r(t_{k+1})\right) + F(t_{k+1}, n, u_n^k),\ k = 0,1,\dots,N-1
\end{cases}
\tag{22}
$$

Under the following assumptions the consistency (of second order) and the convergence are proven in our previous work: *Faragó et al.*, (2013).

Assumption 1 $\partial_3 F : \mathbb{R}^3 \to \mathbb{R}$ *is bounded;* $\partial_3 F \leq F_{max} \in \mathbb{R}$.
Note that a similar assumption is usual in the literature, (see, e.g., *Hoff*, 1978; *Koto*, 2008).
Assumption 2 *The coefficient functions p and q are nonnegative.*
Assumption 3 *For all* $k = 1,2,\dots,N$ *the following inequalities hold true:*

$$
s_1^k = \frac{25}{23}d_1^k - \frac{1}{23}\frac{d_1^k}{d_2^k} - \frac{1}{23}\frac{d_1^k c_2^k}{d_2^k} > 0
$$

$$
s_2^k = \frac{25}{23}c_n^k - \frac{1}{23}\frac{c_n^k}{c_{n-1}^k} - \frac{1}{23}\frac{c_n^k d_{n-1}^k}{c_{n-1}^k} > 0.
$$

Remark: The inequalities in Assumption 3 are equivalent with

$$
\mathbf{25}\boldsymbol{d_2^k} > \mathbf{1} + \boldsymbol{c_2^k} \Leftrightarrow \boldsymbol{r p_2}\left(\mathbf{25}\boldsymbol{q_{\frac{5}{2}}} - \boldsymbol{q_{\frac{3}{2}}}\right) > \mathbf{1}
$$

$$
25c_{n-1}^k > 1 + d_{n-1}^k \Leftrightarrow r p_{n-1}\left(25q_{n-\frac{1}{2}} - q_{n+\frac{1}{2}}\right) > \tag{23}
$$

Lemma 4.1 *The scheme Eq. (22) is consistent with the boundary value problem Eq. (21), and the corresponding order of consistency is* $\mathcal{O}(\tau) + \mathcal{O}(h^2)$.

To rewrite Eq. (22) into a more accessible form we introduce the notations for $j = 1, 2, \ldots, n$:

$$rp_j^k q_{j-\frac{1}{2}}^k = c_j^k \quad \text{and} \quad rp_j^k q_{j+\frac{1}{2}}^k = d_j^k \quad \text{with} \quad r = \frac{\tau}{h^2}.$$

With these we define the matrix

$$\begin{pmatrix} 1+\frac{25}{23}d_1^k & -\frac{26}{23}d_1^k & \frac{1}{23}d_1^k & & 0 \ \ldots \ 0 \\ -c_2^k & 1+c_2^k+d_2^k & -d_2^k & & 0 \ \ldots \ 0 \\ 0 \ -c_3^k & & 1+c_3^k+d_3^k & -d_3^k & \cdots \quad 0 \\ \vdots \ \vdots & & \vdots & \vdots & \ddots \quad \vdots \\ 0 \ \ldots & & 0 & -c_{n-1}^k & 1+c_{n-1}^k+d_{n-1}^k \quad -d_{n-1}^k \\ 0 \ \ldots & & 0 & \frac{1}{23}c_n^k & -\frac{26}{23}c_n^k \quad 1+\frac{25}{23}c_n^k \end{pmatrix}$$

and the vector

$$\boldsymbol{v}^k = \left(\frac{\tau}{h}p_1^k\left(q_{\frac{3}{2}}^k \cdot \frac{1}{23} \cdot u_l(t_k) + q_{\frac{1}{2}}^k u_l(t_k)\right), 0, \ldots, 0, -\frac{\tau}{h}p_n^k\left(q_{n-\frac{1}{2}}^k \cdot \frac{1}{23} \cdot u_r(t_k) + q_{n+\frac{1}{2}}^k u_r(t_k)\right)\right)^T.$$

The time stepping in Eq. (22) then can be given as

$$\boldsymbol{u}^k = A_{k+1,h}\boldsymbol{u}^{k+1} - \tau \boldsymbol{F}(t, h, \boldsymbol{u}^k) + \boldsymbol{v}^{k+1}. \tag{24}$$

The following property of $A_{k,h}$ is of central importance.

Lemma 4.2 *For all* $h > 0$ *and* $k = 0, 1, \ldots, N$ *we have* $\left\|A_{k,h}^{-1}\right\|_\infty = 1$.

Theorem 4.1 *The finite difference method given by Eq. (22) converges to the solution of Eq. (21), and*

$$\max_{j \in \{1,2,\ldots,n\}} \left\|u_j^N - u(T, h_j)\right\| = \mathcal{O}(\tau) + \mathcal{O}(h^2). \tag{25}$$

Proof: The error of the solution in the consecutive time steps is defined as

$$\left(e_1^k,\ e_2^k, \dots, e_n^k\right) = \boldsymbol{e}^k = u(k,\cdot) - u^k.$$

The consistency of the scheme implies that

$$\boldsymbol{u}(k,\cdot) = A_{k+1,h}\boldsymbol{u}(k+1,\cdot) - \tau \boldsymbol{F}\left(t, h, \boldsymbol{u}(k,\cdot)\right) + \boldsymbol{v}_{k+1} - \mathcal{R}^k,$$

where

$$\left\|\mathcal{R}^k\right\|_\infty = \tau(\mathcal{O}(\tau) + \mathcal{O}(h^2)). \tag{26}$$

This, together with Eq. (24) gives that

$$e^k = A_{k+1,h}e^{k+1} - \tau\left(\boldsymbol{F}(t,h,\boldsymbol{u}^k) - \boldsymbol{F}\left(t,h,\boldsymbol{u}(k,\cdot)\right)\right) + \mathcal{R}^k,$$

or in an equivalent form

$$\boldsymbol{u}^k - \boldsymbol{u}(k,\cdot) = e^{k+1} =$$
$$A_{k+1,h}^{-1}\, e^k + \tau A_{k+1,h}^{-1}\left(\boldsymbol{F}(t,h,\boldsymbol{u}^k) - \boldsymbol{F}\left(t,h,\boldsymbol{u}(k,\cdot)\right)\right) + \mathcal{R}^{k+1}.$$

Therefore, using the result in Lemma, the Lagrange inequality, and Assumption 3 we obtain

$$\left\|\boldsymbol{e}^{k+1}\right\|_\infty \le \left\|\boldsymbol{e}^k\right\|_\infty + \tau \boldsymbol{F}_{max}\left\|\boldsymbol{e}^k\right\|_\infty + \left\|\mathcal{R}^{k+1}\right\|_\infty \tag{27}$$

for all $k = 1, 2, \dots, N$. The consecutive application of Eq. (27) gives that

$$\|\boldsymbol{e}^N\|_\infty \le (1 + \tau \boldsymbol{F}_{max})^{N-1}\|\mathcal{R}^1\|_\infty + (1 + \tau \boldsymbol{F}_{max})^{N-2}\|\mathcal{R}^2\|_\infty + \dots + \|\mathcal{R}^N\|_\infty$$
$$\le N(1 + \tau \boldsymbol{F}_{max})^N \max_{j\,\epsilon\,\{1,2,\dots,n\}}\left\|\mathcal{R}^j\right\|_\infty \le T e^{T\cdot F_{max}} \frac{max_{j\,\epsilon\,\{1,2,\dots,n\}}\left\|\mathcal{R}^j\right\|_\infty}{\tau}$$

such that according to Eq. (26) we obtain the estimate in the theorem.

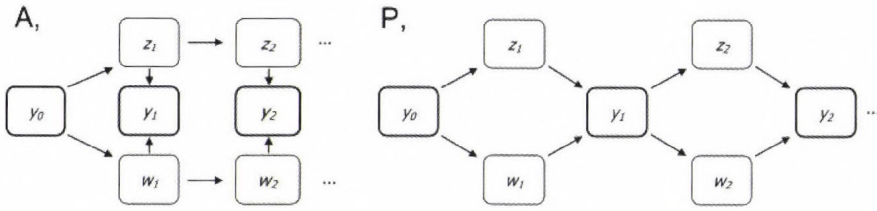

Fig. 2. Schematic comparison of the different Richardson extrapolation procedures: passive method (left) and active method (right)

5. Richardson extrapolation

According to Theorem 3, the previously presented numerical scheme provides us 2nd order of consistency in space, but not in time. We apply the Richardson extrapolation as a powerful device to increase the accuracy of the numerical method in *Richardson*, (1927). In general, it consists of the application of the given numerical scheme. In order to have a 2nd order scheme both in space and time, the application of another mathematical device is crucial.

Richardson extrapolation is a powerful device to increase the accuracy of some numerical method. It consists in applying the given numerical scheme with different discretization parameters (in our case, Δt and $\Delta t/2$) and combining the obtained numerical solutions by properly chosen weights. Namely, if p denotes the order of the chosen numerical method, w_n is the numerical solution obtained by $\Delta t/2$ and z_n that obtained by Δt, then the combined solution

$$y_n = \frac{2^p w_n - z_n}{2^p - 1}$$

has an accuracy of order $p + 1$. This method was first used by L. F. Richardson (*Richardson*, 1927) who called it "the deferred approach to the limit". The Richardson extrapolation is widely used especially for time integration schemes, where, as a rule, the results obtained by two different time-step sizes are combined.

The Richardson extrapolation can be implemented in two different ways when one attempts to increase the accuracy of a time integration method (see Figure 2), namely, passive and active Richardson extrapolations (*Zlatev*, 2010). These two versions of the Richardson extrapolation are also described in (*Botchev* and *Verwer*, 2009), where they are called global and local Richardson

extrapolations. The main difference between these two methods is that in the case of passive extrapolation, the numerical solutions obtained with different step sizes are computed independently of the result of the extrapolation obtained at the previous time step, while in the active version, the result of the extrapolation is used as initial condition in each time step.

Remark 5.1 *It is not difficult to see that if the passive device is applied and the underlying method has some qualitative properties, then the combined method also possesses this property. However, if the active device is used, then this is not valid anymore: any property of the underlying method does not imply the same property of the combined method. Therefore, the active Richardson extrapolation requires further investigation when a given numerical method is applied.*

6. Numerical results

We present some numerical results here corresponding to the model problem discussed in Section 2.3. The analytic and numerical solution are compared at $T = 1$ in *Fig. 3* for a single parameter set.

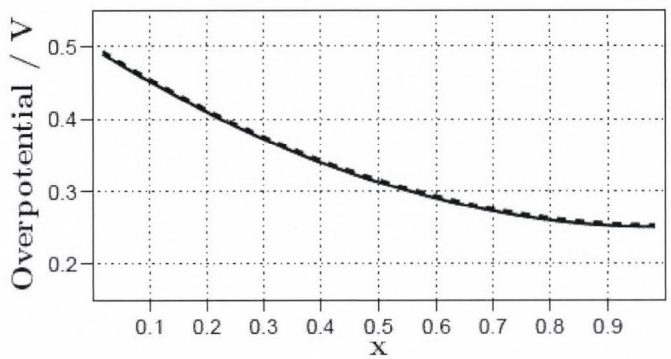

Fig. 3: Analytic solution Eq. (19) of Eq. (12) (continuous line) and the numerical approximation (dashed line) obtained by the method in Eq. (22) with $T = 1$, $N = 25$, and $\tau = 0.01$ for the test problem in Section 2.3. The remaining parameters are given in the Appendix.

We investigated the order of convergence in the $\|\cdot\|_\infty$ norm experimentally with respect to the spatial discretization. To this aim we consecutively refined

the grid and the time step simultaneously such that the ratio $\frac{\tau}{h^2}$ is kept at constant level. Accordingly, in the figures we only investigate the dependence of the $\|\cdot\|_\infty$ -norm error on the number $\frac{1}{h}$ of the spatial grid points. The corresponding results are shown in *Fig. 4*. The numerical results confirm our expectation in Section 4: we can fit accurately a line of slope –2 to the log-log data, which shows a second order convergence with respect to the spatial discretization parameter, see *Fig. 4*.

In *Fig. 5* we illustrated the order of the convergence of the numerical models obtained by the application of the two types of Richardson extrapolation (active and passive) methods. Comparing this result to *Fig. 4*. (i.e., to the results obtained without Richardson extrapolation), one can easily see that the application of these methods led to lower approximation errors. Though, in the case of active Richardson extrapolation, the convergence becomes second order only in the limit $h \to 0$.

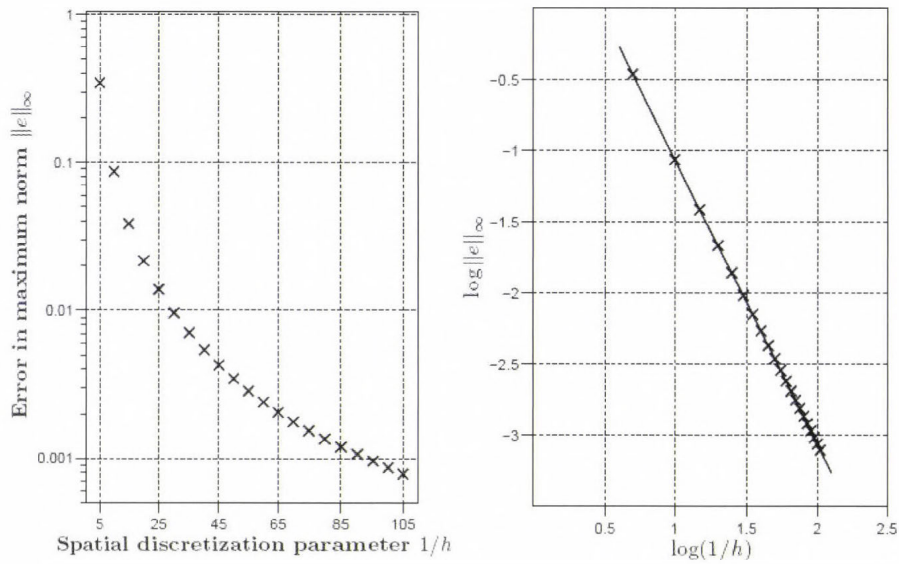

Fig. 4. $\|\cdot\|_\infty$ norm error in the numerical solution (obtained by the presented IMEX method) for the test problem in Section 2.3 vs. the spatial discretization parameter (left). Log-log plot of the error vs. the spatial discretization parameter and a fitted line with slope –2 (right).

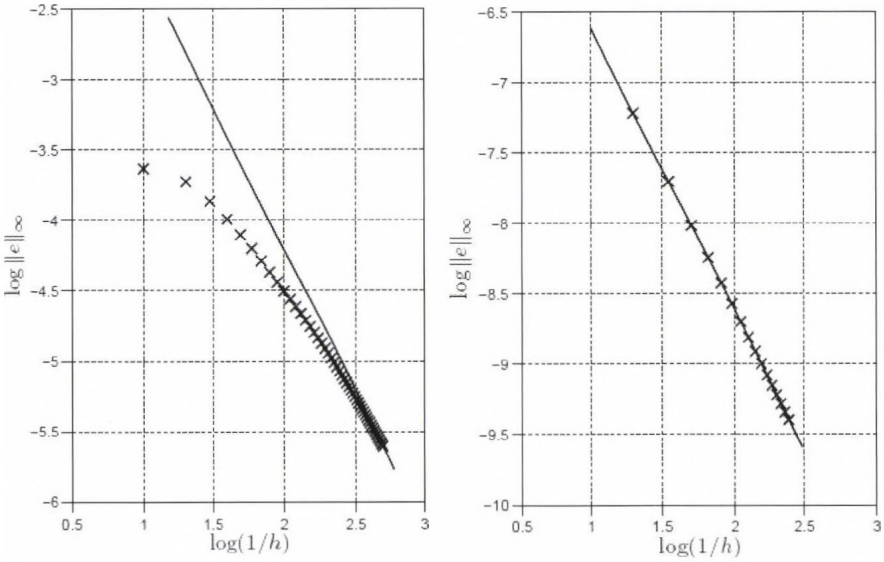

Fig. 5. Log-log plot of the $\|\cdot\|_\infty$ norm error vs. the spatial discretization parameter for the active Richardson extrapolation (left) and the passive Richardson extrapolation (right).

7. Conclusions

Our results have proven that the combination of the presented implicit-explicit method with some Richardson extrapolation methods can be a useful device for solving reaction-diffusion equations numerically. The numerical results in the previous section are also supporting our theoretical analysis.

Aknowledgements–The first author was supported by Hungarian National Research Fund OTKA No. K67819. All authors were supported by the European Union and co-financed by the European Social Fund (grant agreement no. TAMOP 4.2.1./B-09/1/KMR-2010-0003). The Financial support of the National Office of Research and Technology (OMFB-00121-00123/2008) is acknowledged by the authors.

References

Botchev, M.A. and *Verwer, J.G.*, 2009: Numerical integration of damped Maxwell equations. *SIAM J. Sci. Comput. 31(2),* 1322–1346.

Faragó, I.,Izsák, F., Szabó,T., and *Kriston, A.*, 2013: An IMEX scheme for reaction-diffusion equations: application for a PEM fuel cell model., *Cent. Eur. J. Math. 11*, 746–759.

Hoff, D., 1978: Stability and convergence of finite difference methods for systems of nonlinear reaction-diffusion equations. *SIAM J. Numer. Anal. 15*, 1161–1177.

Koto, T., 2008: IMEX Runge-Kutta schemes for reaction-diffusion equations. *J. Comput. Appl. Math., 215*, 182–195.

Kriston, A., Inzelt, G., Faragó, I., and *Szabó, T.*, 2010: Simulation of the transient behavior of fuel cells by using operator splitting techniques for real-time applications. *Comput. Chemical Eng. 34*, 339–348.

Litster, S. and *Djilali, N.*, 2007: Mathematical modelling of ambient air-breathing fuel cells for portable devices. *Electrochimica Acta, 52,* 3849–3862.

Newman, J. and *Thomas-Alyea, K.E.*, 2004: Electrochemical systems. John Wiley & Sons, Inc., Hoboken, New Yersey.

Richardson, L.F., 1927: The deferred approach to the limit, i-single lattice. *Philosophical Transactions of the Royal Society of London 226*, 299–349.

Subramanian, V.R., Boovaragavan, V., and *Diwakar. V.D.*, 2007: Toward real-time simulation of physics based lithium-ion battery models. *Electrochem. Solid-State Lett. 10,* A255–A260.

Ziegler, C., Yu, H.M., and *Schumacher, J.O.*, 2005: Two-phase dynamic modeling of pemfcs and simulation of cyclo-voltammograms. *J. Electrochem. Soc. 152*, A1555–A1567.

Zlatev, Z., Faragó, I., and *Havasi, A.*, 2010: Stability of the Richardson extrapolation applied together with the Θ-method. *J. Comput. Appl. Math. 235*, 507–517.

Appendix

Symbol	Description	Unit
a	Specific interfacial area	cm^{-1}
C_{dl}	Double-layer capacitance	F/cm^2
E_{cell}	Cell potential	V
E_{OC}	Open circuit potential	V
F	Faraday constant (96487)	C/mol
I	Total cell current density	A/cm^2
i_0	Exchange current density at the cathode	A/cm^2
i_0^a	Exchange current density at the anode	A/cm^2
i_1	Solid phase current density at the cathode	A/cm^2
i_2	Solution phase current density at the cathode	A/cm^2
i_f	Faradaic current density	A/cm^3
j_D	Limiting current at the cathode	A/cm^2
L	Thickness of the cathode	cm
R	Universal gas constant (8.3144)	J/molK
T	Cell temperature	K
V^*	Potential loss at the cathode	V
W_{mem}	Membrane thickness	cm
α	Transfer coefficient in the cathode	
α_a^a	Anodic transfer coefficient at the anode	
α_c^a	Cathodic transfer coefficient at the anode	
η	Overpotential at the cathode	V
η^a	Overpotential at the anode	V
ν^2	Dimensionless Exchange current density	
ϕ_1	Solid phase potential	V
ϕ_2	Solution phase potential	V
κ_{eff}	Effective solution phase conductivity	S/cm
σ_{eff}	Effective solid phase conductivity	S/cm
σ_{mem}	Membrane conductivity	S/cm

IDŐJÁRÁS

Quarterly Journal of the Hungarian Meteorological Service
Vol. 117, No. 2, April – June, 2013, pp. 219–237

Projected changes in the drought hazard in Hungary due to climate change

Viktória Blanka[1*], **Gábor Mezősi**[1*], and **Burghard Meyer**[2]

[1]*University of Szeged,*
Egyetem u. 2-6. H-6722 Szeged, Hungary

[2]*Universität Leipzig,*
Ritterstraße 26. DE-04109 Leipzig, Germany

**Corresponding authors E-mails: blankav@geo.u-szeged.hu,*
mezosi@geo.u-szeged.hu

(Manuscript received in final form December 18, 2012)

Abstract–In the Carpathian Basin, drought is a severe natural hazard that causes extensive damage. Over the next century, drought is likely to remain one of the most serious natural hazards in the region. Motivated by this hazard, the analysis presented in this paper outlines the spatial and temporal changes of the drought hazard through the end of this century using the REMO and ALADIN regional climate model simulations.

The aim of this study was to indicate the magnitude of the drought hazard and the potentially vulnerable areas for the periods 2021–2050 and 2071–2100, assuming the A1B emission scenario. The magnitude of drought hazard was calculated by aridity (De Martonne) and drought indices (Pálfai drought index, standardised anomaly index). By highlighting critical drought hazard areas, the analysis can be applied in spatial planning to create more optimal land and water management to eliminate the increasing drought hazard and the related wind erosion hazard.

During the 21st century, the drought hazard is expected to increase in a spatially heterogeneous manner due to climate change. On the basis of temperature and precipitation data, the largest increase in the drought hazard by the end of the 21st century is simulated to occur in the Great Hungarian Plain. Moreover, the changes in the extreme indices (e.g., days with precipitation greater than 30 mm, heat waves, dry periods, wet periods) suggest that the frequency and duration of drought periods will increase. The drought hazard is projected to be lowest in the westernmost part of Hungary. This result is based on qualitative and quantitative analyses that showed the changes in precipitation, temperature, and extreme indices.

Key-words: regional climate change, ALADIN and REMO models, drought hazard, drought indices

1. Introduction

Drought is a severe natural phenomenon that occurs on most of the continents, and it causes extensive damage (*Kogan*, 1997). Drought is one of the most prevalent environmental hazards in parts of Europe and Russia (*Briffa et al.,* 1994, *Meshcherskaya* and *Blazhevich,* 1997). In the Carpathian Basin, drought is one of the most severe natural hazards, causing serious damage to the national economy, agriculture, and water resources. The lack of water during drought periods is harmful for all living organisms, including humans, and can result in social and economic consequences, such as drinking water shortages and reductions in agricultural yields.

Despite the seriousness of this phenomenon, drought is not a well-defined term, and the technical and colloquial uses of this term vary greatly. The absence of a precise and universally accepted definition of drought can lead to confusion concerning whether a drought exists and what the severity is. This imprecision causes considerable debate among meteorologists, farmers, and public officials. Researchers use the term "drought" to describe periods when precipitation is below average, leading to water shortages, and unmet demand for water (*Vermes et al.*, 2000). Drought is a creeping phenomenon. It is often difficult to ascertain when a drought begins, as the deficiency of moisture in a region takes time to emerge (*Changnon*, 1987), and when it ends (*Warrick et al.,* 1975). In addition to precipitation, a number of factors play a significant role in the evolution of a drought. These factors include evaporation, which is affected by temperature and wind, soil type and its ability to store water, the depth and presence of groundwater supplies, and vegetation. Accounting for these factors, three types of droughts are commonly noted: meteorological (*Palmer,* 1965, *Farago et al.,* 1989), agricultural (*Maracchi,* 2000), and hydrological (*Pálfai*, 2002a; *Hisdal* and *Tallaks*en, 2003). In addition, the terms "drought" and "aridification" are often confused. It is important that drought be distinguished from aridification. Generally, drought is described as a temporary phenomenon (*Dracup et al.*, 1980), while aridification is described as the process of a region becoming increasingly dry.

Due to the discrepancies in describing these phenomena (differing definitions of event duration and numerous measurement methods – *Heim,* 2002), researchers often apply numerical methods or indices (e.g., the Palmer index, Standardised precipitation index (SPI), De Martonne index, and the Pálfai aridity index (PAI)) to define drought-affected areas (*Svoboda et al.*, 2002; *Dunkel,* 2009). The application of these indices can eliminate the uncertainty of estimating the spatial and temporal extent and severity of a drought.

In the Carpathian Basin, drought is a severe natural hazard that causes extensive damage, and it is regarded as the most prominent natural hazard of the next century (*Bakonyi*, 2010). Therefore, the aim of this study was to outline the spatial and temporal changes in the drought hazard until 2100 by using

experiments of the REMO and ALADIN regional climate models. These model simulations are suitable for this analysis because they use the A1B scenario (*Nakicenovic* and *Swart,* 2000), which represents intermediate estimations for the changes in greenhouse gas emissions over the next century, to model anthropogenic forcing. These model experiments have been used successfully in previous climate studies (*Szépszó* and *Horányi,* 2008; *Csima* and *Horányi,* 2008; *Pieczka et al.,* 2010; *Rannow et al.* 2010; *Mezősi et al.* 2012).

These models predicted a continuous, but not constant temperature increase in the Carpathian Basin, with the most intense increase occurring in the summer months (the rate of change is similar to that experienced between 1980 and 2010). The change in annual precipitation simulated by model experiments is not significant; however, the distribution of precipitation within a year is likely to change more significantly, the decreasing summer and increasing winter precipitation would result more homogenous distribution of the precipitation throughout the year (*Tables 1* and *2*) (*Bartholy et al.,* 2008; *Szabó et al.,* 2010; *Csorba et al.* 2012).

Table 1. Changes in the projected mean annual and seasonal temperature (°C) compared with the mean from the period of 1961–1990 based on the REMO and ALADIN model experiments (*Szabó et al.,* 2010)

Period	Year	Spring	Summer	Autumn	Winter
2021–2050	(+1.4)–(+1.9)	(+1.1)–(+1.6)	(+1.4)–(+2.6)	(+1.6)–(+2.0)	+1.3
2071–2100	+3.5	(+2.3)–(+3.1)	(+4.1)–(+4.9)	(+3.6)–(+3.8)	(+2.5)–(+3.9)

Table 2. Changes in the projected mean annual and seasonal precipitation (%) compared with the mean from the period of 1961-1990 based on the REMO and ALADIN model experiments (*Szabó et al.*, 2010)

Period	Year	Spring	Summer	Autumn	Winter
2021-2050	(–1)– 0	(–7)–(+3)	–5	(+ 3)–(+14)	(–10)–(+7)
2071–2100	(–5)–(+3)	(–2)–(+2)	(–26)–(–20)	(+10)–(+19)	(–3)–(+31)

Climate simulations show that extreme climate events may occur more frequently in the Carpathian Basin over the next century, and that more prolonged and severe hot and dry periods are projected. The number of frost days could decrease by 30 % by 2050 and by 50 % by the end of the 21st century, and the number of summer days (T_{max}>25 °C) could become double or

even triple the present number (*Szépszó,* 2008). The projection for precipitation involves more uncertainty, in certain seasons even the tendency is contradictory in the REMO and ALADIN model simulations (*Szabó et al.,* 2010). Uncertainties in these long-term climate simulations arise from the nearly unpredictable social and economic changes that may occur over the next century and from the internal variability of the climate system (*Bartholy* and *Pongrácz,* 2010). However, despite the prediction limitations, this analysis can provide valuable information for future environmental and spatial planning (*Mezősi et al.*, 2012).

The aim of this study is to predict the magnitude of the drought hazard and the potentially vulnerable areas in Hungary for the periods 2021–2050 and 2071–2100, assuming the A1B emission scenario. This analysis can be used to highlight the critical drought areas. This information can be considered in spatial planning to create more optimal land and water management and to eliminate the increasing drought hazard and the related wind erosion hazard. These hazard projections can become an integral part of drought planning, preparedness, and mitigation efforts at the national, regional and local levels.

2. Methods

2.1. Determination of the landscape units

Due to the resolution of the climate data, an analysis of the 230 traditional, environmentally homogeneous micro-regions of Hungary were not possible; therefore, 18 larger landscape units were defined (*Fig. 1*). The areas of the defined units are better suited to the resolution of the climate data and the demands of spatial planning. The determination of the landscape units was based on the spatial diversity of landscape shaping factors (relief, soil, geology, vegetation, land use, and climate). The borders of the units were matched to the shapes of larger natural landscape units (e.g., micro-regions along the middle and lower sections of the Tisza River) and economic regions (e.g., central Hungary), where the border was justified by the climate dependence of the land use.

Due to their small areas, these landscape units are not substantive climatically. However, the physical parameters are relatively homogeneous in the units; therefore, any climate change affects the entire unit in the same way. An analysis on this scale can be important for the recognition of probable future climate effects and in the development of strategic spatial plans.

1 Little Hungarian Plain
2 Western part of the Carpathian Basin
3 Zala Hills
4 Marcal basin and Komárom Plain
5 Transdanubian Mountains
6 Hilly region of Inner Somogy
7 Transdanubian Hills
8 Dráva Plain and Mecsek Mountains
9 Mezőföld Plain
10 Danubian Plain
11 Danube-Tisza Interfluve
12 Gödöllő Hills
13 Western part of the North Hungarian Mountains
14 Eastern part of the North Hungarian Mountains
15 Plain of Upper Tisza
16 Plains of Nyírség and Hajdúság
17 Central part of the Great Hungarian Plain
18 Körös-Maros Interfluve

Fig. 1. The examined landscape units (after *Csorba et al.*, 2012)

2.2. Calculation of the climate data

The simulated future changes of the climate parameters were analyzed using two regional climate models, REMO and ALADIN. The models utilize the A1B scenario, which represents the average changes of greenhouse gas emissions, to model anthropogenic climate forcing. The A1B scenario describes an integrated world with rapid economic growth, slowing population increases, a quick spread of new and efficient technologies, and a balanced emphasis on all energy sources (*Nakicenovic* and *Swart,* 2000). The resolution of the climate data was 0.22 ° (approximately 25 km). The climate projections were generated by the Numerical Modelling and Climate Dynamics Division of the Hungarian Meteorological Service.

Daily temperature and precipitation data for the periods 2021–2050 and 2071–2100 were used in the calculations. The temperature and precipitation data

changes are in °C and mm, respectively, with respect to the reference period of 1961–1990. The following changes in the extreme climate indices were also generated from the two models: frost days in days/year; summer days (T_{max}>25 °C) in days/year; extremely heavy precipitation days ($R_{day} \geq 30$ mm), in days/year; and the simple daily intensity index (SDII), which is a measure of the precipitation amount per rainy day ($R_{day} \geq 1$ mm), in mm/day. From all of these data, average yearly and monthly data were calculated and evaluated for the two study periods. Regional average values were calculated for the landscape units based on the climate parameters at each grid point.

2.3. Assessing the change in drought hazard

One method of evaluating drought hazard is calculating drought or aridity indices. Several indices use only precipitation and temperature data, while others evaluate the soil moisture condition or water budget and may be recursive (e.g., the widely known and frequently used Palmer index). All of these indices have advantages and disadvantages; therefore, comprehensive studies generally apply a number of indices to obtain a better result by eliminating the deficiencies of a single index (e.g., the US Drought Monitor uses seven different indices).

During this research, two different methods were applied to assess the future changes in the drought hazard and associated results. A qualitative analysis was applied to define the tendencies of the changes, and a quantitative analysis was used to provide numerical values for the changes.

In the qualitative analysis, the future climate change trends were assessed, and the current probability of drought occurrence in the landscape units was analyzed using the PAI (*Pálfai*, 1984, 1990, 2002b). The present-day conditions were compared with the tendencies due to climate change. The tendencies caused by climate change and the regions with similar characteristics were identified by cluster analysis. The temperature and precipitation data and 4 extreme climate indices (average number of summer days, average number of frost days, average number of heavy precipitation days - with precipitation above 20 mm, and the SDII precipitation index, describing number of precipitation days – above 1 mm rainfall) were used in the cluster analysis. After extracting the factor coefficients for the regions, hierarchical clustering applied, where natural groupings can be detected. Cluster analysis of the factors coefficients gave an alternative linkage approaches and metrics. The assessment identified the sensitivity of the landscape units and the vulnerable areas. This method did not provide information about the magnitude of the changes, but it took more parameters into account than did the aridity and drought indices. This result means that a more complex description of the changes can be provided that considers which extreme climate indices enhance or eliminate the effect of mean temperature and precipitation changes.

To evaluate the magnitude of the changes, aridity and drought indices were calculated. For the investigation, three indices with different temporal resolutions and that were determined through different calculation methods were selected. The indices were calculated by using observed meteorological data of the reference period (1961–1990) and the projected changes of the model simulations. This method of choosing indices reduced the errors from the models and allowed differences within a year to be estimated.

2.4. Aridity index: De Martonne (IDM)

To begin, an aridity index was calculated. Aridity indices primarily characterize the climate of a region rather than the drought hazard. However, as aridity increases, the occurrence of drought can become more frequent and the severity can grow, thereby increasing the drought hazard. From among several aridity indices, the De Martonne index was selected, which is based on annual temperature and precipitation data.

De Martonne index (*IDM*):

$$IDM = P/(T+10),$$

where P is the annual precipitation and T is the annual mean temperature. The temporal resolution of the input data is low, but this index is widely used (*Doerr,* 1963; *Botzan et al.,* 1998; *Grieser,* 2006; *Paltineanu et al.,* 2007; *Baltas,* 2007; *Livada* and *Assimakopoulos,* 2007; *Lungu et al.*, 2011). It was observed that the index properly demonstrates the spatial differences of drought.

The future drought hazard can be estimated by calculating drought indices. These indices were developed to describe the drought level on annual and sub-annual timescales. In this study, average values for the 30-year periods (2021–2050 and 2071–2100) was calculated, therefore, the drought levels in individual years could be notably different in the landscape units. Due to the uncertainties in the climate projections, it is not advisable to calculate the indices for shorter periods. In addition, a long-term average value showing the tendency of the change can be more applicable for spatial planning purposes.

2.5. Drought indices: $PaDI_0$ and the standardized anomaly index (SAI)

Two drought indices were calculated, the $PaDI_0$ index and the standardized anomaly index (*SAI*). The $PaDI_0$ index uses monthly temperature and precipitation data, and average monthly data were evaluated for the two study periods (*Pálfai* and *Herceg*, 2011). The $PaDI_0$ is based on the *PAI* and is used in Hungary, but its simplicity allows for wider use. Both $PaDI_0$ and *PAI* is a relative

indicators that characterize the drought with one numerical value that is associated with one agricultural year.

$PaDI_0$ index:

$$PaDIo = \frac{\left[\sum_{i=apr}^{aug} Ti\right] / 5 * 100}{\sum_{i=oct}^{sept} (Pi * wi)},$$

where T_i is the mean monthly temperature from April to August, P_i is the monthly sum of precipitation from October to September, and w_i is a weighting factor (*Table 3*). The weighting factor expresses the importance of the months in the evolution of drought. The $PaDI_0$ index characterizes a drought with one numerical value for one agricultural year. The index focuses on the drought occurring in the vegetation period, as is indicated by the monthly weighting factors. The index was developed in Hungary, and it reveals the drought periods particularly well under the climatic conditions of the Carpathian Basin.

Table 3. Weighting factors w_i of monthly precipitation in $PaDI_0$ (*Pálfai* and *Herceg*, 2011)

Month	Weight factor (w_i)	Month	Weight factor (w_i)
October	0.1	April	0.5
November	0.4	May	0.8
December	0.4	June	1.2
January	0.5	July	1.6
February	0.5	August	0.9
March	0.5	September	0.1

To describe the role of precipitation changes in the changing drought hazard, an index was calculated using only precipitation data. The SAI was used to characterise the precipitation variability in a particular region. The main advantage of this index is the low data demand; however, in some situations, it does not indicate the drought level correctly (*Katz* and *Glantz,* 1986, *McKee et al.*, 1993). Generally, the index is calculated for shorter periods (from 1 to 12 months), but it was computed for the two 30-year periods in this case. Even when calculated over longer periods, the SAI produces acceptable temporal and spatial differences in the drought hazard. For this evaluation, three-month SAI values were calculated for the most drought-prone and agriculturally important period, from June to August.

SAI:

$$SAI = \frac{P - m(P)}{d(P)},$$

where P is the precipitation amount, $m(P)$ is the average precipitation of the reference period, and $d(P)$ is the standard deviation of the precipitation in the reference period (1960–1990).

These indices provide numerical values of the changes in the drought hazard even though they analyse only a few parameters. These indices do not provide the most accurate value for the drought hazard because they use only the temperature and precipitation data (they do not even use evaporation or groundwater level data). However, all of the input data are extractable from the applied climate models. The aim of this study was not to give an accurate value of future changes in the drought hazard but to show the tendencies on the meso-scale.

3. Results

3.1. *Qualitative analysis of the future drought hazard*

The *PAI* (*Pálfai*, 2004) shows that the highest drought level was located in the landscape unit of the Great Hungarian Plain, and it decreased toward the north and west. The highest *PAI* values were in the central and southern part of the Great Hungarian Plain. The lowest values were in the higher elevations of the Alpokalja region and on the higher hills of the North Hungarian Mountains (*Fig. 2*).

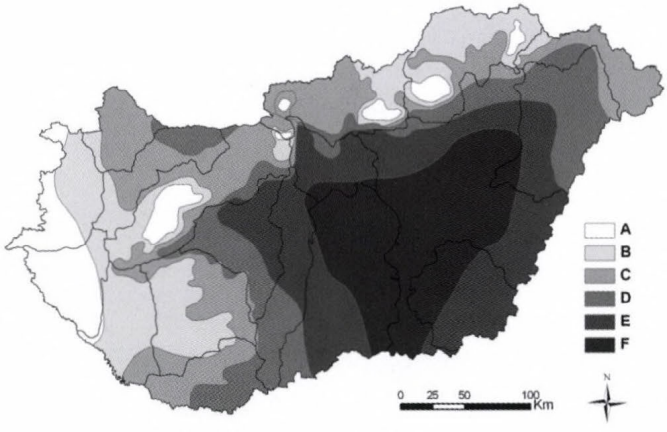

Fig. 2. Drought map of Hungary (*Pálfai*, 2004) (A: drought free; B: mild; C: moderate; D: medium; E: high; F: extremely high rate of exposure).

Despite the small area and the relatively low topographic diversity of the region, the two climate simulations showed spatial differences in the parameters. Four regions in Hungary with different climate change tendencies were defined by a cluster analysis based on the temperature, precipitation and extreme indices. In these regions, the climate change tendencies indicated diverse alterations of the social and ecological systems. The climate change in the 21st century affects the drought hazard differently in each of the four regions (*Mezősi et al.*, 2012).

The climate change tendencies in these regions have similar characteristics. The region type 1 is located along a west central corridor ranging from north to south. Moderate temperature increases and distinct changes in extreme temperature events are projected. Future precipitation is projected to increase with higher rates but moderate changes in extreme rainfall events. The region type 2 covers the northeastern regions along the Slovakian border. This region had the lowest annual mean temperatures and the highest intraregional temperature variation. Moderate future increases are simulated with moderate increases in the number of extreme event days. The region type 3 is essentially the Hungarian Great Plain, excluding the Plains of Nyírség and Hajdúság regions. This region has the highest temperatures and the lowest annual precipitation totals. The region is projected to experience the highest temperature increases, greatest changes in extreme temperature events (increases in summer days and decreases in frost days), highest precipitation decline ratios (or at least the lowest precipitation increase ratios), and an increase in the number of heavy rainfall days. The region type 4 covers only two landscape units in the western hilly area. This type is characterized by smaller temperature increases and smaller changes in temperature extremes. This region type is simulated to be more humid and have higher precipitation totals, smaller precipitation change ratios, and smaller change rates with regard to heavy rain events (*Fig. 3*).

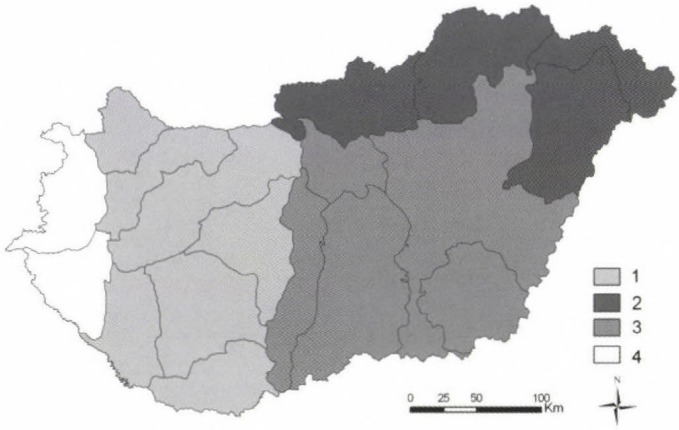

Fig. 3. Regional types of climate change exposure as a result of cluster analysis (*Mezősi et al.*, 2012).

The increase in the annual mean temperature affects the increase in the drought hazard in all regions. The largest increase in the drought hazard by the end of the 21st century is simulated in the third region type, because the increase in the annual mean temperature, increase in the number of summer days, and decrease in precipitation will all be the largest in this region type. Moreover, the increase in the number of extremely heavy precipitation days and the SDII indicated that the precipitation will fall in a more concentrated time period, which suggests that the frequency and duration of drought periods will increase. Additionally, this region already has the highest drought hazard.

In the first and second region types, the temperature increases are also projected to be significant, but the precipitation change will be slight, with a possible small increase. A moderate increase in the drought hazard is projected. The highest precipitation total and the lowest annual mean temperature currently occur in the fourth region, and future changes are projected to be moderate. The drought hazard will be the lowest in this region (*Fig. 4*).

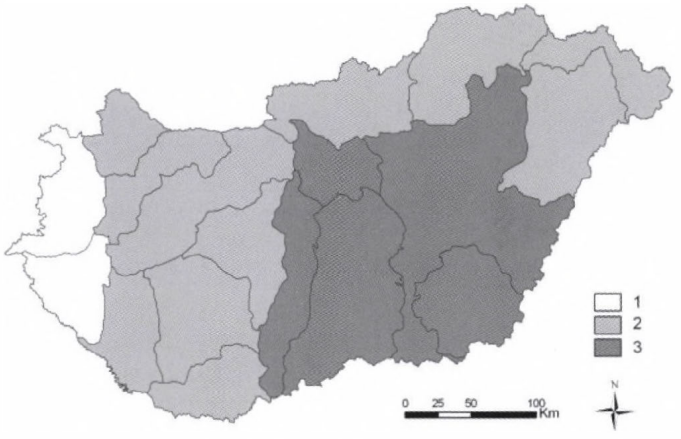

Fig. 4. Future changes in drought hazard due to climate change in the regions with similar characteristics (1. slight increase; 2. moderate increase; 3. major increase).

By using the regions defined by a cluster analysis as a basis for the analysis, the spatial differences and relations between the climate change tendencies and the changes in the drought hazard were revealed. Verification of the results is problematic, but the uncertainties can be reduced by using different calculation methods. Accordingly, the magnitude of the changes and the spatial differences were also analyzed by calculating the De Martonne index, $PaDI_0$ index, and SAI.

4. *Quantitative analysis of the future drought hazard*

4.1. Changes in the De Martonne index

In the reference period (1961–1990), the value of the De Martonne index varied between 23.7 mm/°C and 33.5 mm/°C in the landscape units on the basis of observed meteorological data. The lowest values, representing the highest aridity, were observed in the southeastern part of Hungary. The landscape units in that region of the country (the Danube-Tisza Interfluve and Körös-Maros Interfluve) were categorized as mediterranean (20 mm/°C $\leq$ IDM $\leq$ 24 mm/°C). The largest part of the country was categorized as semi-humid (24 mm/°C $\leq$ IDM $\leq$ 28 mm/°C), while some units along the northeastern and western borders were categorised as humid (28 mm/°C $\leq$ IDM $\leq$ 35 mm/°C).

Changes in the drought hazard can be analyzed with categories from the De Martonne index, which defines the drought hazard as low in humid regions, moderate in semi-humid regions, and high in mediterranean regions. Any future changes in the De Martonne index indicate changes in the drought hazard. For the period 2021–2050, the two model simulations showed similar changes; namely, the index values are likely to decrease to 20.7–31.4 mm/°C and 20.7–31.0 mm/°C using REMO and ALADIN outputs, respectively. In the southeastern and central regions of Hungary, four landscape units were transferred to the mediterranean category, and the Nyírség and Hajdúság units were transferred to the semi-humid category. For the period 2071–2100, the value of the index is projected to decrease in all of the units; however, the difference between the model experiments is larger in this period (19.6–28.8 mm/°C in case of REMO and 18.2–27.3 mm/°C in case of ALADIN). In the ALADIN model, the landscape unit of the Great Hungarian Plain, except for the Plains of Nyírség and Hajdúság portions, was transferred to the semi-dry (10 mm/°C $\leq$ IDM $\leq$ 20 mm/°C) category. When using outputs of REMO simulation, the spatial distribution of the changes was similar. However, this model indicated less significant changes, and only the Körös-Maros Interfluve unit was transferred to the semi-dry category. The index values also decreased in the humid-category landscape units in the two model simulations, and the units were transferred to the semi-humid category when using outputs of ALADIN simulation. Consequently, the De Martonne index indicates a future increase in the drought hazard over the entire country by 2100. The ALADIN model predicts that the changes will be more pronounced, and that all units will transfer at least one category to a more arid type by 2100. The REMO model showed less pronounced changes, and category changes were typical only in the northern part of the country and in the Hungarian Great Plain. In the Hungarian Great Plain, a new category is likely to appear, namely the semi-dry category, which indicates a very large drought hazard (*Fig. 5*).

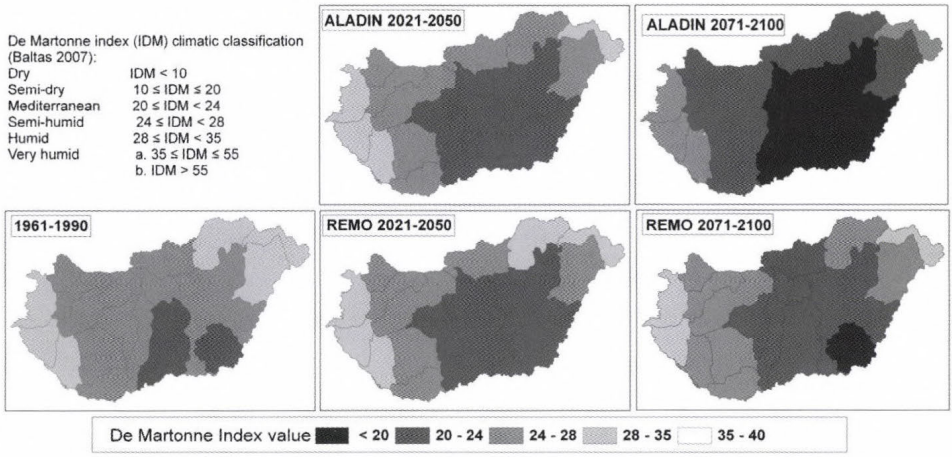

Fig. 5. Values of the De Martonne index in the periods of 1961–1990, 2021–2050, and 2071–2100.

4.2. Changes in the $PaDI_0$ index

The average value of the $PaDI_0$ index for the base period (1961–1990) varied between 3.5 and 5.3 °C/100 mm in the landscape units. These values are lower than those of the PAI (shown in *Fig. 2*). Because the calculation of the $PaDI_0$ was made for distinct years and averaged over 30 years, the extremes are hidden. Nevertheless, this result still correctly predicts the temporal changes. The maximum values of the index, which represent the highest drought hazard, were obtained in the landscape units in the central part of Hungary (the Gödöllő Hills, Danube-Tisza Interfluve, and the Danubian Plain). In contrast, the lowest values occurred in the western part of the country; therefore, the drought hazard was the lowest here.

The changes in the drought hazard can be analyzed using the changes in the drought-level categories of the $PaDI_0$ as a proxy. For the period 2021–2050, both model simulations indicated that the value of the index will increase, varying between 3.9 and 6.0 °C/100 mm (in case of REMO) and between 3.9 and 6.5 °C/100 mm (in case of ALADIN). The highest degree of change was indicated in the southeastern part of Hungary. Using REMO outputs, the maximum values are simulated in the Danube-Tisza Interfluve and Körös-Maros Interfluve units. Using ALADIN outputs, the maximum values are projected in the Körös-Maros Interfluve unit and in the central part of the Great Hungarian Plain unit (*Fig. 6*).

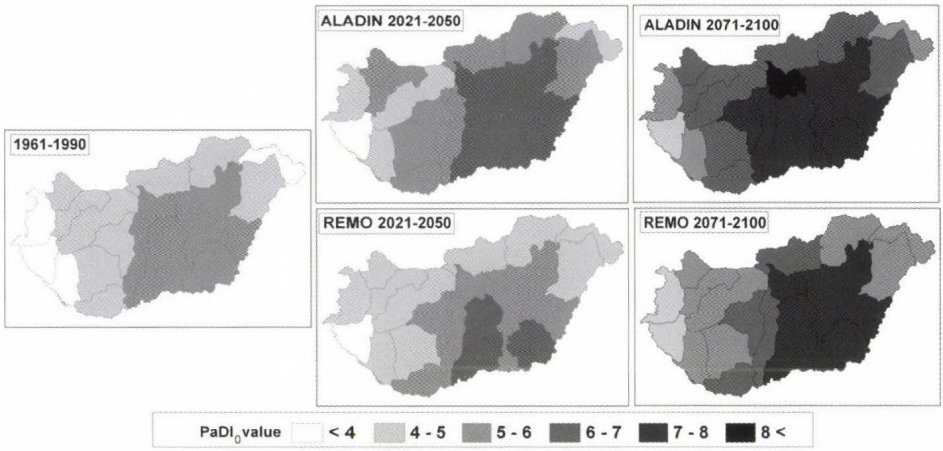

Fig. 6. Values of the $PaDI_0$ index in the periods of 1961-1990, 2021-2050, and 2071-2100.

For the period 2071–2100, the drought hazard is projected to increase, but significant differences were recognized between the model simulations (4.7–7.5 °C/100 mm and 4.8–8.4 °C/100 mm using REMO and ALADIN outputs, respectively). According to the REMO model, the maximum values are simulated in the Körös-Maros Interfluve unit and the central part of the Great Hungarian Plain unit. The predicted value of the index based on the ALADIN model is expected to exceed the highest values of the REMO model in the Gödöllő Hills unit.

4.3. Changes in the SAI

Changes in the precipitation were analyzed using the SAI for the three summer months (June to August), when the drought hazard is the highest.

According to the three-month SAI, the drought hazard is not projected to change significantly (the value varied between –1 and 1) until the 2021–2050 period, although there is notable uncertainty in these results considering the differences between the two model simulations. The model simulations indicate different rates of change, and in the northern and western parts of Hungary, the trend of the changes was different. A considerable increase in the drought hazard is simulated only in the southeastern part of Hungary, where both model simulations indicate the same tendency (*Fig. 7*).

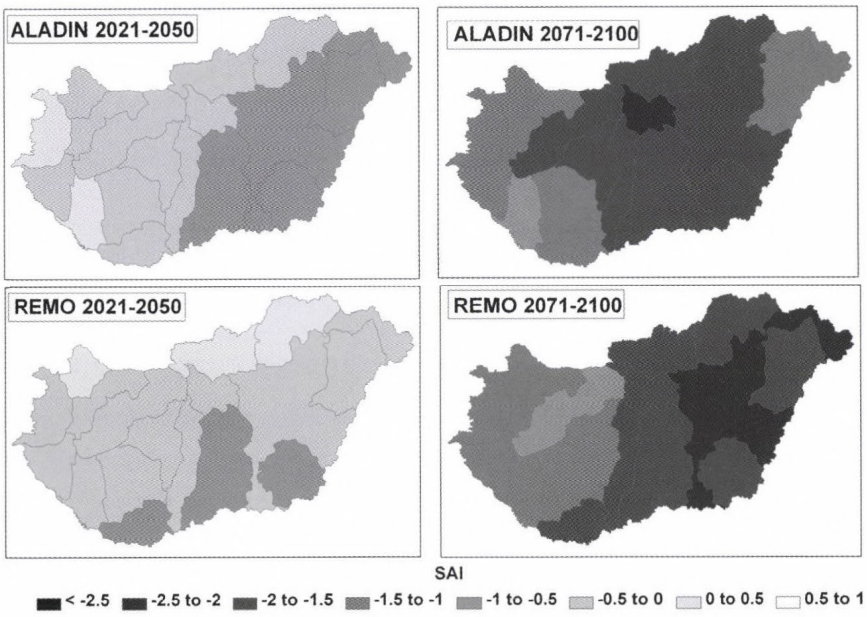

Fig. 7. Values of the SAI in the periods of 2021-2050 and 2071-2100

Both model simulations have clearly indicated an increase in the drought hazard in the summer months for the entire country by the end of the 21st century. Even despite the uncertainty of the precipitation projection, the value of the SAI varied between –0.5 and –2.5 in the period 2071–2100. The highest rate of precipitation decrease, with respect to the base period (1961–1990), is simulated in the northern part of the Great Hungarian Plain and the North Hungarian Mountains. However, due to the more favorable initial conditions in the North Hungarian Mountains, the drought hazard will be less serious even with large changes. The most critical drought hazard projected in all of the landscape units is in the north central part of the Great Hungarian Plain. The value of the SAI is below –2 in this unit, which indicates extreme dryness.

5. Conclusion

During the 21st century, the drought hazard in Hungary is likely to increase in a spatially heterogeneous manner due to climate change. The future changes in the drought hazard were assessed using two approaches, namely a qualitative and quantitative analysis. The two approaches provided similar results for the changes in the drought hazard. These assessments showed that the drought hazard is expected to increase throughout the country but with spatially different

magnitudes. The maximum increase in the drought hazard is projected in the five landscape units of the Hungarian Great Plain. According to the qualitative analysis, the future tendency of the changes in the precipitation, temperature, and extreme indices is the most severe in terms of drought level in these units. The quantitative analysis confirmed these results. The most intensive changes in the calculated indices are likely to occur in the same landscape units. For these five units, the initial value and the amount of increase in the $PaDI_0$ were the highest, and the SAI value were the lowest in the country. The maximum change in the De Martonne index is likely to occur in these units, but, due to the initial conditions, the highest drought hazard is simulated in these units by the end of the 21st century.

By 2021–2050 period, the increase in the drought hazard is projected to be not significant. However, the results from the ALADIN simulations showed that the drought hazard is likely to increase in the landscape units of the Hungarian Great Plain, while the results from the REMO simulations indicated a significant increase only in the two southernmost units of the Hungarian Great Plain. These two landscape units currently have the highest drought hazard, causing climate change to generate severe drought problems in these units first. By 2071–2100 period, both model experiments indicated a significant drought hazard increase in all units of the Hungarian Great Plain. The results showed that the Körös-Maros Interfluve unit is projected to have the worst drought hazard. The De Martonne index was found to be highest on the basis of both model simulations for this unit, and the results from the REMO simulations showed that the $PaDI_0$ index was the highest. The *SAI*, based only on precipitation data, indicated that the most severe drought hazard is simulated in the Gödöllő Hills and the central part of the Great Hungarian Plain, but this index does not consider temperature changes. In the Gödöllő Hills, the results from the ALADIN simulations showed that the $PaDI_0$ index indicated the most intense drought hazard. This indicated that, despite the smaller temperature increases, the intense precipitation changes in the summer months are likely to cause severe water supply problems in this area.

According to the qualitative and quantitative analyses, the westernmost part of Hungary is likely to have the lowest drought hazard due to favorable changes in the precipitation, temperature, and extreme indices in this region.

This analysis, based on climate simulation data, suggests that the drought hazard will increase in the entire country, and that the most intense changes are simulated in the Hungarian Great Plain, which is currently the most drought-affected area. The Körös-Maros Interfluve and the Gödöllő Hills are particularly vulnerable. In these areas, more serious drought problems are projected to occur by the end of the 21st century than at present. The modification of drought hazards can be a slow process, but future strategies and landscape planning should include the development of mitigation strategies and preparations for environmental damage.

The drought hazard projections have several uncertainties. The most important uncertainties are the lack of verification and an accurate definition of the error. Further uncertainty is associated with the A1B scenario, as the projected data are only valid for a definite socio-economic development path. Despite these limitations, the present data set and analysis of the smaller units can provide valuable data for several sectors of society, including the economy, as the analysis can highlight the critical drought areas. This information can promote the development of optimal spatial planning strategies to create more optimal land and water management, which can mitigate the consequences of drought at national, regional and local levels. Preparing for prospective droughts by developing optimal land use and water management plans is a key objective of spatial planning to mitigate the damage caused by droughts

Additionally, these calculations consider only climate parameters, while other environmental parameters (e.g., the water-holding capacity of soils, groundwater depth and wind conditions) should be taken into consideration to obtain a more detailed and accurate definition of the drought hazard. The positive or negative characteristics of these parameters can locally modify the drought hazard.

The positive or negative characteristics of these parameters can locally modify the drought hazard. Therefore, further analysis is required to reveal how the drought hazard influences the complex interrelationship between the soil water, salinity of the soil and soil water, groundwater depth, land use, land cover, or local relief situation.

Acknowledgement–The research was funded by the „TÁMOP-4.2.1/B-09/1/KONV-2010-0005 – Creating the Center of Excellence at the University of Szeged" and the TÁMOP-4.2.2/B-10/1-2010-0012 – "Broadening the knowledge base and supporting the long-term professional sustainability of the Research University Centre of Excellence at the University of Szeged by ensuring the rising generation of excellent scientists" projects supported by the European Union and co-financed by the European Regional Fund.

References

Bakonyi, P., 2010: Flood and drought strategy of the Tisza river basin. VITUKI, Budapest, www.icpdr.org/icpdr-files/15494

Baltas, E., 2007: Spatial distribution of climatic indices in northern Greece. *Meteorol. Appl.14*, 69–78.

Bartholy, J. and *Pongrácz, R.*, 2010: Analysis of precipitation conditions for the Carpathian Basin based on extreme indices in the 20th century and climate simulations for the 21st century. *Phys. Chem. Earth 35*, 43–51.

Bartholy, J., Pongrácz, R., Gelybó, Gy., and *Szabó,* P., 2008: Analysis of expected climate change in the Carpathian Basin using the PRUDENCE results. *Időjárás 112*,249–264.

Botzan, M.A., Marino, M.A., and *Necula, A.I.*, 1998: Modified de Martonne aridity index: Application to the Napa Basin, California. *Phys. Geogr. 19*, 55–70.

Briffa, K.R., Jones, P.D., and *Hulme, M.*, 1994: Summer moisture variability across Europe, 1892–1991: an analysis based on the Palmer drought severity index. *Int. J. Climatol. 14*, 475–506.

Changnon, S.A., 1987: Detecting drought conditions in Illinois: Illinois State Water Survey, Champaign, Illinois, USA , Circular 169: 1–36.

Csima, G. and *Horányi, A.*, 2008: Validation of the ALADIN-Climate regional climate model at the Hungarian Meteorological Service. *Időjárás 112*, 155–177.

Csorba, P., Blanka, V., Vass, R., Nagy, R., Mezősi, G., and *Meyer, B.* 2012: A hazai tájak működésének veszélyeztetettsége új klímaváltozási előrejelzés alapján (Sensitivity of the Hungarian mesolandscapes according to the modelled climate change). *Földr. Közl.136*, 237–253.

Doerr, A.H., 1963: De Martonne's Index of Aridity and Oklahoma's Climate. *Proc. of the Oklahoma Academy of Science 43*, 211–213.

Dracup, J.A., Lee, K.S., and *Paulson, E.G.* 1980: 'On the definition of droughts', *Water Resour. Res. 16*, 297–302.

Dunkel, Z., 2009: Brief surveying and discussing of drought indices used in agricultural meteorology. *Időjárás 113*, 23–37.

Farago, T., Kozma, E., and *Nemes, Cs.*, 1989: Drought indices in meteorology. *Időjárás 93*, 45–59.

Grieser, J., Gommes, R., Cofield, S., and *Bernardi, M.* 2006: Data sources for FAO worldmaps of Koeppen climatologies and climatic net primary production FAO - The Agromet Group, SDRN. http://www.juergen-grieser.de/downloads/Koeppen-Climatology/CommonData/CommonData.pdf

Heim, R.R., 2002: A review of Twentieth-Century drought indices used in the United States. *B. Am. Meteorol. Soc. 83*, 1149–1165.

Hisdal, H. and *Tallaksen, L.M.*, 2003: Estimation of regional meteorological and hydrological drought characteristics. *J. Hydrol. 281*, 230–247.

Katz, R.W. and *Glantz, M.H.*, 1986: Anatomy of a rainfall index. *Mon. Weather Rev. 114*, 764–771.

Kogan, F.N., 1997: Global Drought Watch From Space. *B. Am. Meteorol. Soc. 78*, 621–636.

Livada, I. and *Assimakopoulos, V.D.*, 2007: Spatial and temporal analysis of drought in Greece using the Standardized Precipitation Index (SPI). *Theor. Appl. Climatol. 89*. 143–153.

Lungu, M., Panaitescu, L.., and *Niţă, S.* 2011: Aridity, climatic risk phenomenon in Dobrudja. *Pres. Environ. Sustain. Develop. 5*, 179–189.

Maracchi, G., 2000: Agricultural Drought – A practical approach to definition, assessment and mitigation strategies. In: *Vogt, J.V., Somma, F.*: Drought and Drought Mitigation in Europe. Advances in Natural and technological hazards Research, 14, Kluwer Academic Publisher Dordrecht, 63–78.

McKee, T.B, Doeskin, N.J., Kleist, J. 1993: The relationship of Drought Frequency and Duration to Time Scales. Proc. 8th Conf. on Applied Climatology. American Meteorological Society, Boston, 179–184.

Meshcherskaya, A.V. and *Blazhevich, V.G.*, 1997: The drought and excessive moisture indices in a historical perspective in the principal grain-producing regions of the Former Soviet Union. *J. Climate 10*, 2670–2682.

Mezősi, G., Meyer, B. C., Loibl, W., Aubrecht, C., Csorba, P., and *Bata, T.* 2012: Assessment of regional climate change impacts on Hungarian landscapes. *Reg. Environ. Change 17/4* online first (7 July 2012)

Nakicenovic, N. and *Swart, R., (eds.)*, 2000: Emissions Scenarios. A Special Report of IPCC Working Group III. Cambridge University Press, Cambridge, UK. 570p. Available at http://www.ipcc.ch/pdf/special-reports/emissions_scenarios.pdf

Pálfai, I. 1984: Az aszályosság index. Magyar Hidrológiai Társaság V. Országos Vándorgyűlés III. kötet 19–24. (In Hungarian)

Pálfai, I. 1990: Description and forecasting of droughts in Hungary. *Transactions of 14th Congress on Irrigation and Drainage. Rio de Janeiro ICID, 1-C*, 151–158.

Pálfai, I. 2002a: Probability of drought occurence in Hungary. *Időjárás 106*, 265–275.

Pálfai, I. 2002b: Magyarország aszályossági zónái. *Vízügyi Közl. 84*, 323-357.

Pálfai, I. 2004: Belvizek és aszályok Magyarországon. Köz Doc, Budapest.

Pálfai, I. and *Herceg, Á.*, 2011: Droughtness of Hungary and Balkan Peninsula. *Riscuri si Catastrofe, An X* 9, 145–154.

Palmer, W.C., 1965: Meteorological Drought. Research Paper No.45, U.S. Department of Commerce Weather Bureau, Washington, D.C., USA.

Paltineanu, C., Mihailescu, I .F., Seceleanu, I., Dragota, C., and *Vasenciuc F.* 2007: Using aridity indices to describe some climate and soil features in Eastern Europe: a Romanian case study. *Theor. Appl. Climatol. 90*, 263–274.

Pieczka, I., Pongrácz, R., Bartholy, J., Kis, A., and *Miklós, E.* 2010: A szélsőségek várható alakulása a Kárpát-medence térségében az ENSEMBLES projekt eredményei alapján. *36. Meteorológiai Tudományos Napok*, OMSZ, Budapest, 76–86. (in Hungarian)

Rannow, S., Loibl, W., Greiving, S., Gruehn, D., and *Meyer, B.C.,* 2010: Potential impacts of climate change in Germany – identifying regional priorities for adaptation activities in spatial planning. *Landscape Urban Plan. 98*,160–171.

Svoboda, M., LeComte, D., Hayes, M., Heim, R., Gleason, K., Angel, J., Rippey B., Tinker, R., Palecki, M., Stooksbury, D., Miskus, D., and *Stephens, S.,* 2002: The Drought Monitor. *B. Am. Meteorol. Soc. 83*, 1181–1190.

Szabó, P., Horányi, A., Krüzselyi, I., and *Szépszó, G.*, 2010: Az Országos Meteorológiai Szolgálat regionális klímamodellezési tevékenysége: ALADINClimate és REMO. *36. Meteorológiai Tudományos Napok*, OMSZ, Budapest, 87–101 (In Hungarian)

Szépszó, G. 2008: Regional change of extreme characteristics over Hungary based on different regional climate models of the PRUDENCE project. *Időjárás 112*, 265–284.

Szépszó, G. and *Horányi, A.,* 2008: Transient simulation of the REMO regional climate model and its evaluation over Hungary *Időjárás 112,* 203–231.

Vermes, L., Fésűs, I., Nemes, C., Pálfai, I., and *Szalai, S.,* 2000: Status and progress of the national drought mitigation strategy in Hungary. In (*Eds: Vermes, L., Szemessy, Á.*) Proceedings of the Central and Eastern European Workshop on Drought Mitigation 12-15 April, Budapest-Felsőgöd, Hungary, 55–64.

Warrick, R.A., Trainer, P.B., Baker, E.J., and *Brinkman, W.* 1975: Drought Hazard in the United States: A Research Assessment NSF Program on Technology, Environment and Man Monograph NSF-RA-E-75-004.

INSTRUCTIONS TO AUTHORS OF *IDŐJÁRÁS*

The purpose of the journal is to publish papers in any field of meteorology and atmosphere related scientific areas. These may be

- research papers on new results of scientific investigations,
- critical review articles summarizing the current state of art of a certain topic,
- short contributions dealing with a particular question.

Some issues contain "News" and "Book review", therefore, such contributions are also welcome. The papers must be in American English and should be checked by a native speaker if necessary.

Authors are requested to send their manuscripts to

Editor-in Chief of IDŐJÁRÁS
P.O. Box 38, H-1525 Budapest, Hungary
E-mail: journal.idojaras@met.hu

including all illustrations. MS Word format is preferred in electronic submission. Papers will then be reviewed normally by two independent referees, who remain unidentified for the author(s). The Editor-in-Chief will inform the author(s) whether or not the paper is acceptable for publication, and what modifications, if any, are necessary.

Please, follow the order given below when typing manuscripts.

Title page: should consist of the title, the name(s) of the author(s), their affiliation(s) including full postal and e-mail address(es). In case of more than one author, the corresponding author must be identified.

Abstract: should contain the purpose, the applied data and methods as well as the basic conclusion(s) of the paper.

Key-words: must be included (from 5 to 10) to help to classify the topic.

Text: has to be typed in single spacing on an A4 size paper using 14 pt Times New Roman font if possible. Use of S.I. units are expected, and the use of negative exponent is preferred to fractional sign. Mathematical formulae are expected to be as simple as possible and numbered in parentheses at the right margin.

All publications cited in the text should be presented in the *list of references*, arranged in alphabetical order. For an article: name(s) of author(s) in Italics, year, title of article, name of journal, volume, number (the latter two in Italics) and pages. E.g., *Nathan, K.K.,* 1986: A note on the relationship between photo-synthetically active radiation and cloud amount. *Időjárás 90,* 10-13. For a book: name(s) of author(s), year, title of the book (all in Italics except the year), publisher and place of publication. E.g., *Junge, C.E.,* 1963: *Air Chemistry and Radioactivity.* Academic Press, New York and London. Reference in the text should contain the name(s) of the author(s) in Italics and year of publication. E.g., in the case of one author: *Miller* (1989); in the case of two authors: *Gamov* and *Cleveland* (1973); and if there are more than two authors: *Smith et al.* (1990). If the name of the author cannot be fitted into the text: *(Miller,* 1989); etc. When referring papers published in the same year by the same author, letters a, b, c, etc. should follow the year of publication.

Tables should be marked by Arabic numbers and printed in separate sheets with their numbers and legends given below them. Avoid too lengthy or complicated tables, or tables duplicating results given in other form in the manuscript (e.g., graphs).

Figures should also be marked with Arabic numbers and printed in black and white or color (under special arrangement) in separate sheets with their numbers and captions given below them. JPG, TIF, GIF, BMP or PNG formats should be used for electronic artwork submission.

Reprints: authors receive 30 reprints free of charge. Additional reprints may be ordered at the authors' expense when sending back the proofs to the Editorial Office.

More information for authors is available: journal.idojaras@met.hu

Published by the Hungarian Meteorological Service

Budapest, Hungary

INDEX 26 361

HU ISSN 0324-6329